frontiers in Ecology and Evolution

ORIGINAL RESEARCH
published: 25 February 2019
doi: 10.3389/fevo.2019.00044

Reconstruction of the Early Miocene Critical Zone at Loperot, Southwestern Turkana, Kenya

Cynthia M. Liutkus-Pierce[1], Kevin K. Takashita-Bynum[2], Luke A. Beane[1], Cole T. Edwards[1], Oliver E. Burns[1], Sara Mana[3], Sidney Hemming[4], Aryeh Grossman[5], James D. Wright[6] and Francis M. Kirera[7]*

[1] Department of Geological and Environmental Sciences, Appalachian State University, Boone, NC, United States, [2] Watershed Institute, Murray State University, Murray, KY, United States, [3] Department of Geological Sciences, Salem State University, Salem, MA, United States, [4] Lamont Doherty Earth Observatory, Columbia University, Palisades, NY, United States, [5] Department of Anatomy, Midwestern University, Glendale, AZ, United States, [6] Department of Earth and Planetary Science, Rutgers University, New Brunswick, NJ, United States, [7] School of Medicine, Mercer University, Macon, GA, United States

The Hominoidea (apes and, eventually, humans) and Cercopithecoidea (Old World monkeys) diverged from a common ancestor during the late Oligocene (~25 Ma) in East Africa. Subsequently, both catarrhine groups diversified in the early Miocene (~23-16 Ma), making this time period an extremely important one for understanding our (deep) ancestral roots and the link between our hominoid ancestors and the environment. A remote region of west Turkana known as Loperot provides an exciting opportunity to study early Miocene primate paleoecology and has the potential to reveal the phylogenetic relationship between cercopithecoid monkeys and stem hominoids. The site of LpM4 is particularly fossiliferous and has produced a diverse fauna that includes several catarrhine fossils that await description. Radioisotopic dating indicates that the Loperot fauna are older than ~17 Ma (early Miocene). Using geochemical data from paleosols and stable isotope values from rhizolith calcite, coupled with detailed sedimentology and stratigraphy, we reconstruct the early Miocene Critical Zone of Loperot to reveal a large perennial river system fed by ephemeral streams that created localized riparian forest microhabitats within a larger open ecosystem under semi-arid climate conditions, making Loperot's environmental reconstruction unlike many other early Miocene catarrhine-bearing localities. The perennial river system supported corridors of C_3 forests; however, because these forests were restricted, they could not support a high diversity of forest indicator taxa. This is the most comprehensive analysis of the environmental conditions at Loperot to date, and provides new empirical evidence to suggest that African climate varied significantly by region and that arid habitats certainly existed during the early Miocene.

Keywords: Miocene, Loperot, Kenya, Critical Zone, cattarhine, paleosol

OPEN ACCESS

Edited by:
Florent Rivals, Catalan Institution for Research and Advanced Studies, Spain

Reviewed by:
Manuel Hernández Fernández, Complutense University of Madrid, Spain
Ferran Estebaranz-Sánchez, University of Barcelona, Spain
Naomi E. Levin, University of Michigan, United States

****Correspondence:***
Cynthia M. Liutkus-Pierce
liutkuscm@appstate.edu

Specialty section:
This article was submitted to Paleoecology, a section of the journal Frontiers in Ecology and Evolution

Received: *11 September 2018*
Accepted: *05 February 2019*
Published: *25 February 2019*

Citation:
Liutkus-Pierce CM, Takashita-Bynum KK, Beane LA, Edwards CT, Burns OE, Mana S, Hemming S, Grossman A, Wright JD and Kirera FM (2019) Reconstruction of the Early Miocene Critical Zone at Loperot, Southwestern Turkana, Kenya. Front. Ecol. Evol. 7:44. doi: 10.3389/fevo.2019.00044

INTRODUCTION

Hominoidea (apes, and eventually humans) and Cercopithecoidea (Old World monkeys) diverged from a Last Common Ancestor during the late Oligocene (~25 Ma) in East Africa (Stevens et al., 2013). Cercopithecoid monkeys, while rare, are easily recognized in the early Miocene fossil record (Miller et al., 2009); by contrast, separating the earliest crown-Hominoids from a large

(20+ species) group (Rossie and Seiffert, 2006) of ape-like stem-Hominoids is difficult. The rarity of early Miocene cercopithecoids, the crucial group necessary for resolving the phyletic relationships of early Miocene stem-hominoids (Rossie and Seiffert, 2006), has led most researchers to either exclude cercopithecoids (Begun et al., 1997) or incorporate middle Miocene *Victoriapithecus macinnesi* into their phylogenetic analyses (Rossie and Seiffert, 2006).

Mammalian assemblages of the early Miocene, including catarrhine primates (the Hominoidea and Cercopithecoidea), differ regionally in their taxonomic structure. Geographic location (Grossman et al., 2014) as well as varying environmental conditions among regions (affected by climate, tectonics, etc.) certainly helped shape mammal assemblage structure (Andrews and O'Brien, 2010; Lukens et al., 2017). Understanding the influence of each of these biotic and abiotic factors on early Miocene primate distribution and abundance requires analysis of the Critical Zone (Brantley et al., 2007; Nordt and Driese, 2013; Lukens et al., 2017) through a synergistic investigation of geology and paleontology.

Dixey (1944) first noted Miocene fossils at Loperot in West Turkana, Kenya (**Figure 1**). A Harvard team began collecting there in 1963–64 (Mead, 1975) and discovered the rhinoceros, *Chilotheridium patersoni* (Hooijer, 1971), the oldest shovel-tusked proboscidean from Africa, *Platybelodon* sp. (Maglio, 1969), and a ziphiid whale (Mead, 1975; Wichura et al., 2015). Among the primates recovered is one molar attributed to *Limnopithecus legetet* (Harrison, 1982) and two (as yet) undescribed molars of a cercopithecoid. In 1989, Meave Leakey recovered two more monkey specimens, which also await description. Our team began excavations in 2012, and our research has added the hyrax, *Meroehyrax* sp., and the giraffid, *Canthumeryx* sp. (Grossman et al., 2014) to the faunal list. We also recovered several primate specimens that are currently being analyzed and described.

Loperot's age and catarrhine presence makes it perfectly suited to provide crucial data for recognizing the first crown-Hominoid and placing an early Miocene catarrhine assemblage from western Turkana in paleoenvironmental context. While we await the analysis of the primate fossils, here we reconstruct the early Miocene Critical Zone at site LpM4 from Loperot to gain an understanding of the climatic and environmental conditions during this crucial time in primate evolution through complimentary analyses of the sedimentology, stratigraphy, paleontology, and paleosol geochemistry.

BACKGROUND AND GEOLOGIC SETTING

The Early Miocene Environment in East Africa

Paleoenvironmental reconstructions vary among early Miocene catarrhine sites in their quantity, quality, and methodologies. In a foundational study, Andrews and Van Couvering (1975) used multiple lines of evidence to show that general climate of the early Miocene in East Africa was warm with relatively high amounts of precipitation. They argue that because the formation of the East African Rift System and associated elevation of the Kenyan and Ethiopian Highlands were yet to occur, the lowland tropical forest today covering most of equatorial West and Central Africa extended eastward during the early Miocene, as far as the coast of Kenya. They reconstruct extensive bands of tropical woodland extending both south and north of the equatorial forest zone at that time. For example, they say that the sites of Rusinga and Mwafangano Islands were within the tropical lowland zone along with Koru, Songhor, and Napak, while the sites of Loperot and Moruorot were located in the woodland zone north of the lowland equatorial forest zone. These same authors also recognize that elevation of certain volcanoes, specifically Tinderet, could lead to the formation of a montane forest within the lowland forest zone and suggest that this occurred at Songhor. They add that two hypothesized river systems, one in what is modern day Winam Gulf (=Kavirondo Gulf), and a second, suggested by a fossil whale at Loperot, drained West-East rather than North-South. This West-East drainage system could have created local barriers affecting animal dispersal patterns in East Africa, possibly explaining some of the differences between sites associated with the Kisingiri volcano (e.g., Rusinga) and the Tinderet volcano (e.g., Songhor). However, they emphasize that even within an overall tropical forest zone, one should not assume that local conditions are necessarily forested, as seen by different localities at Rusinga Island (Andrews and Van Couvering, 1975). Although it is likely that overall temperatures were relatively warm and stable during the early Miocene in East Africa, sites indeed differ locally in annual rainfall and degree of seasonality (Peppe et al., 2017). (See **Supplemental Information** for a brief review of other early Miocene paleoenvironmental reconstructions to date).

The Lokichar Basin

Loperot (western Turkana) is known for its abundant fossiliferous strata and has been studied since the 1940s (Dixey, 1944; Maglio, 1969; Hooijer, 1971; Mead, 1975; Wichura et al., 2015). The site is located on the western side of modern day Lake Turkana, a rift lake within the East African Rift System situated between the Kenyan and Ethiopian domes (Morley et al., 1999a; Feibel, 2011; **Figure 1A**). During the early Miocene, the Loperot region experienced uplift and subsequent erosion, followed by an extended period of extension along NW-SE striking normal faults (Joubert, 1966). Episodes of volcanic activity intercalated Miocene sediment with numerous tuffs and basalts before another erosional event during the Pliocene (Joubert, 1966). Numerous rift basins, including the Lokichar Basin, formed due to Tertiary normal faulting (Feibel, 2011).

Loperot sits within the Lokichar Basin, which is separated from the neighboring Kerio Basin by a topographic high of Precambrian basement called the Lokone Horst (Hendrie et al., 1994; Morley et al., 1999b). The basin is a 60 km long by 30 km wide, north-south trending half graben bounded by an east-dipping border fault on the west side (Morley et al., 1999b; **Figures 1B**, **2A**). Over 7 km of sediment fill the Lokichar Basin (Feibel, 2011), and pollen analysis indicates Eocene through late Miocene strata beneath the Auwerwer Basalt (Joubert, 1966; Boschetto et al., 1992; Morley et al., 1999a; **Figure 2B**).

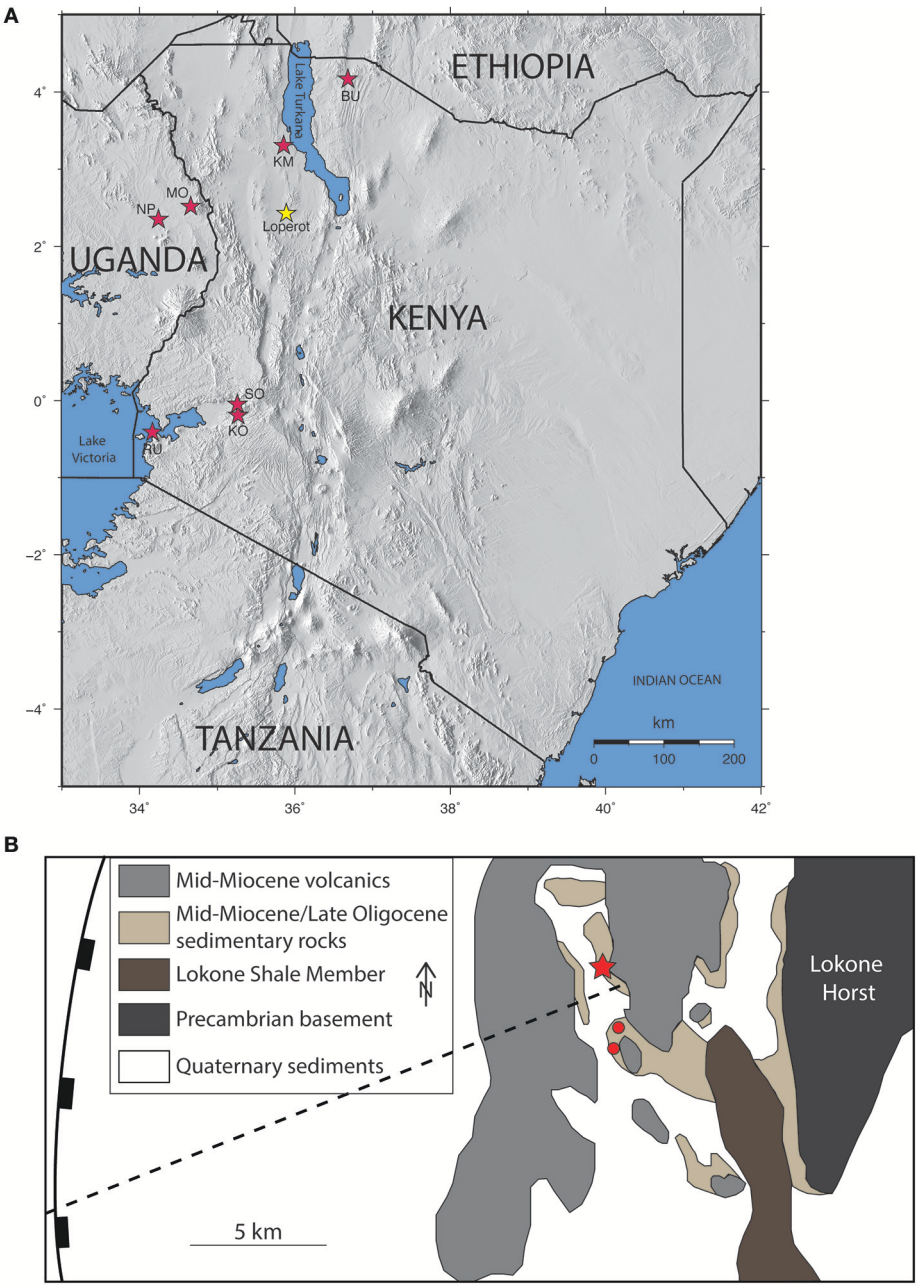

FIGURE 1 | (A) Regional map of East Africa, showing the location of Loperot (west Turkana) in relation to other important Miocene catarrhine sites, including Rusinga Island (RU), Koru (KO), Songhor (SO), Napak (NP), Moroto (MO), Kalodirr and Moruorot (KM), and Buluk (BU). **(B)** Detailed geologic map of the Lokichar Basin, showing exposed Oligocene and Miocene deposits to the west of the Lokone Horst and to the east of the border fault; modified from Morley et al. (1999b). Dashed line indicates the cross-section shown in **Figure 2A**. Red star denotes site LpM4; red dots identify the locations of sites LpM2 (southern) and LpM3 (northern).

Regional Stratigraphy

The sediment infill of the Lokichar Basin below the Auwerwer Basalts was known previously as the Turkana Grits (Joubert, 1966) and are now subdivided into the Lokone and Auwerwer Sandstone Formations (Morley et al., 1999b; **Figure 2B**). The Lokone Formation (Paleogene to early Miocene) has an unconformable basal contact with Precambrian basement and consists of fluviodeltaic, arkosic sandstones intercalated with two lacustrine shale units (the older Loperot Shale Member and the younger Lokone Shale Member; Morley et al., 1999b). Fluvial and lacustrine environments are inferred based on the presence of crocodile, turtle, oyster, and fish fossils within these sedimentary units (Joubert, 1966; Feibel, 2011). The Auwerwer Sandstone Formation (middle Miocene) sits above the Lokone Formation, is

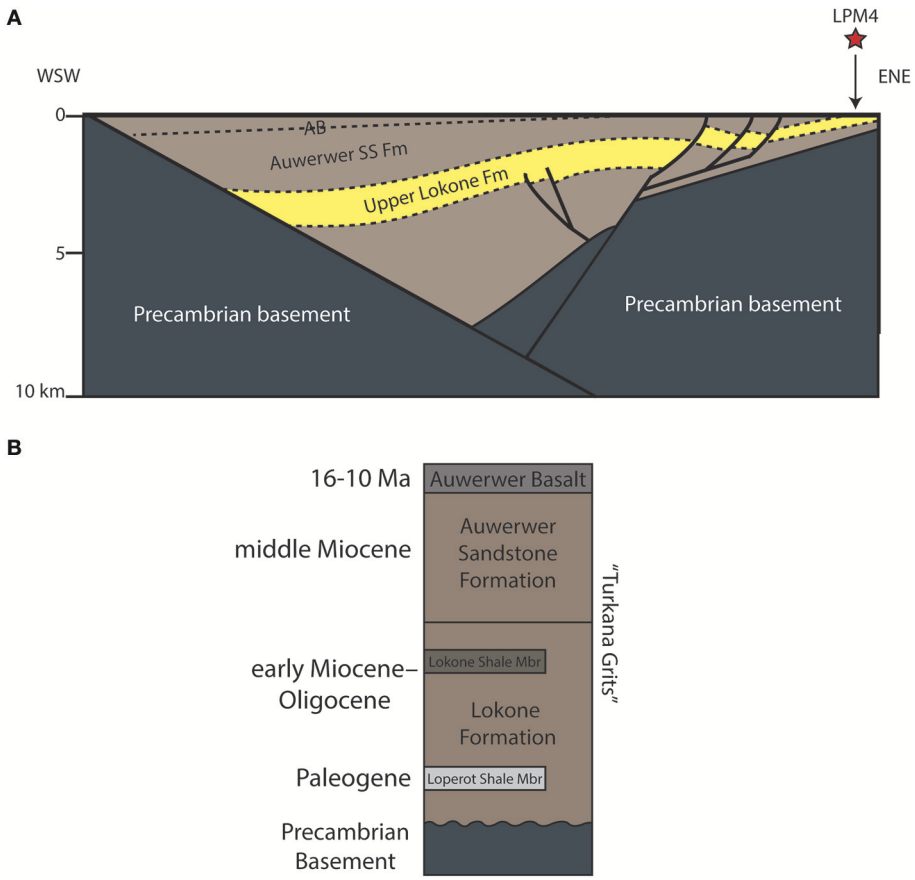

FIGURE 2 | Geology and stratigraphy of the Lokichar Basin. **(A)** Cross-section of subsurface geology of the Lokichar Basin, interpreted from seismic data presented in Morley et al. (1999b). The upper Lokone Formation is highlighted, and due to the half-graben geometry of the basin, it reaches the surface to the east nearest the Lokone uplift. **(B)** Generalized stratigraphy of the Lokichar Basin, modified from Morley et al. (1999b).

of fluviodeltaic origin, and contains less feldspar and considerable volcaniclastic sediment, including reworked tuffs (Morley et al., 1999b). Tiercelin et al. (2004) noted that, in some places, the Auwerwer Sandstone Formation is deficient in volcanic material beneath the Auwerwer Basalt, possibly signifying a change in the sediment source. The ∼300 m-thick Auwerwer Basalt directly overlies the Auwerwer Sandstone Formation and has been radiometrically dated to 16-10 Ma (Morley et al., 1999b).

MATERIALS AND METHODS

Field Methods

Fieldwork enabled the location of several fossiliferous sites near Loperot, identified as LpM2, LpM3, and LpM4 (**Figure 1B**), however only site LpM4 had any appreciable outcrop exposure that allowed for investigation of stratigraphic change through time. Therefore, the results presented here represent data collected from site LpM4, though we report that sites LpM2 and LpM3 are also fossiliferous and warrant future research. In 2016, we excavated a 28 m step-trench at LpM4 (**Figure 3**) and recognized 30 stratigraphic units based on color, lithology, and grain size; additional stratigraphic sections were measured from outcrop (e.g., Exposures 1 and 2) but were not formally trenched (**Figure 3**). Stratigraphic units were measured, described, and compared to previous descriptions (see Morley et al., 1999b) and bulk sediment samples (∼500 mL) were taken from each unit for grain size and bulk geochemical analyses. Field description of paleosol units followed the procedure of Retallack (1990) and color descriptions follow the Munsell Soil Color Chart (Munsell Color, 2010). Recognized paleosol units were subsampled (∼100 mL) at either 10 cm increments or 50 cm increments, depending on the overall thickness of and/or observed variation within the paleosol units.

Laboratory Methods

Radiometric Dating

Two basalt samples representing the same stratigraphic horizon and overlying the ∼28 m-thick sedimentary section studied here were collected ∼20 m apart for ^{40}Ar-^{39}Ar dating (sample LpM4-left1D and sample LpM4-right3A). The samples were crushed with a steel jaw rock crusher and dry sieved. The 25- to 40-mesh split was thoroughly washed with deionized water and sonicated for 20 min. Grains were hand-picked under a binocular microscope, to concentrate fine groundmass without visible

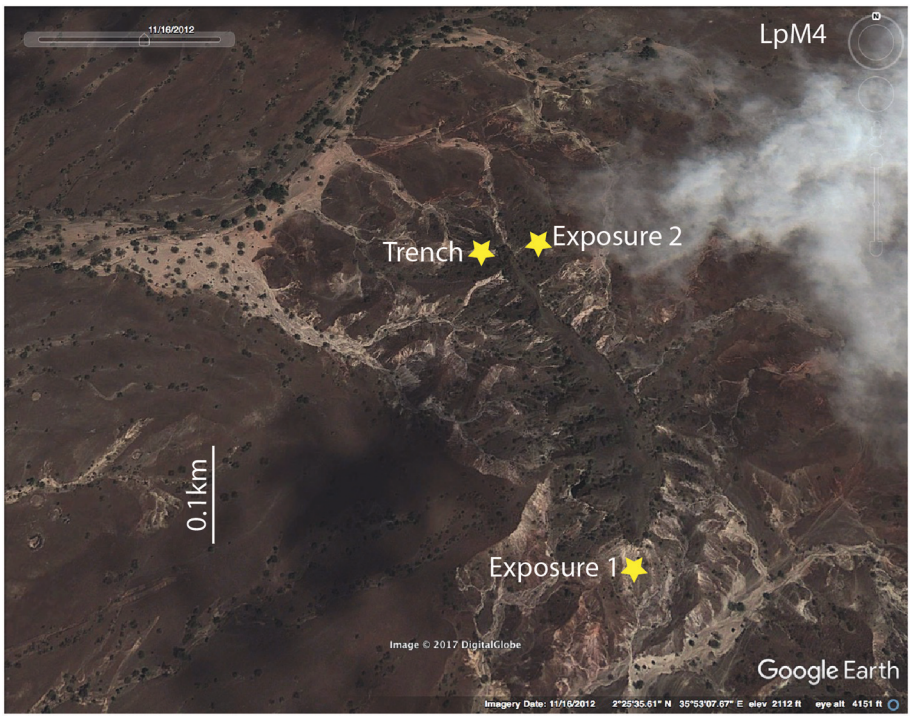

FIGURE 3 | Location of fossil-bearing sites at Loperot's site LpM4. Satellite image of exposures that were excavated, measured, and described (Trench) as well as those that were only described from outcrop (Exposure 1, and Exposure 2). (Map data ©2017 Digital Globe: "LpM4." 22°5′ 35.81″N 35°53′7.67″E. DigitalGlobe, GoogleEarth. 2/25/2017).

crystals or alteration, and co-irradiated for 8 h with Fish Canyon sanidine (28.201 ± 0.046 Ma; Kuiper et al., 2008) at the USGS TRIGA reactor in Denver, CO (USA). Groundmass samples were packaged in Ta-tubes, and incrementally heated using a PhotonMachines 50-watt diode laser at progressively higher power. The released argon was measured on a VG5400 noble gas mass spectrometer at Lamont Doherty Earth Observatory by peak hopping into an analog multiplier. Age calculations were made using the current accepted decay constants of Min et al. (2000), consistent with the Fish Canyon age determination from Kuiper et al. (2008) and isotopic abundances of Steiger and Jager (1977). Measured isotope data were corrected for background contributions and mass discrimination effects based on frequent measurements of backgrounds, air aliquots, and nuclear interference values characteristic of the reactor employed (Dalrymple et al., 1981).

Grain Size and Optical Microscopy

Samples were analyzed for grain size distribution following the procedure of (Lewis and McConchie, 1994) to produce sand/silt/clay ratios. Bulk samples were submerged in acetic acid (15%) to remove carbonate cement, then wet-sieved through a 4-phi sieve to isolate the sand fraction (which was dried and weighed). The remaining silt and clay fractions was suspended in a 1L settling column with 1g of sodium hexametaphosphate and analyzed via the pipette method (Lewis and McConchie, 1994). Size fractions were examined under an optical microscope to identify grain texture and mineralogy.

X-Ray Diffraction

Bulk mineralogy of all sediment samples was determined using X-ray diffraction (using a random unoriented powder pack method) on a Shimadzu XRD6000 operated at 40 kV and 30 mA at Appalachian State University. Bulk samples were ground to a fine powder in a diamonite mortar and pestle, packed into an aluminum slide, and analyzed 10°-80° two-theta using a CuKα beam of wavelength 1.5418 Å. Oriented mounts were made in order to analyze clay mineralogy using the extraction method described by Moore and Reynolds (1997) and the clay-film transfer method discussed by Drever (1973). The air-dried oriented mounts were analyzed from 2° to 32° two-theta, and then exposed to ethylene glycol vapor for at least 24 h, allowed to equilibrate outside the glycolation chamber for 1 h, and then analyzed again on the X-ray diffractometer (2°-32° two-theta).

Rhizolith Size and Stable Isotope Geochemistry

Calcite rhizoliths were collected from within the trench and at Exposure 1 at LpM4 (**Figure 3**). Rhizolith-bearing layers from Exposure 1 were correlated to unit numbers within the trench based on stratigraphic position and facies characteristics. Digital calipers were used to measure the length and width of each rhizolith.

Samples selected for stable isotopic analysis were broken in half to reveal a flat cross-section across the short axis. A Foredom microdrill with a 0.5 mm drill tip was used to collect powdered carbonate material across the entire diameter of each rhizolith. Stable carbon and oxygen isotope ratios were measured at Washington University in St. Louis. Approximately 100 μg of carbonate powder was dissolved in 100% H_3PO_4 for 4 h at 72°C in He-flushed, sealed tubes. Evolved CO_2 was sampled with a Finnigan Gas Bench II and isotopic ratios were measured with a Delta V Plus mass spectrometer. Isotopic data are reported in per mil (‰) using delta notation ($\delta^{13}C$ and $\delta^{18}O$) relative to the Vienna Pee Dee Belemnite standard (V-PDB). Isotopic measurements were calibrated against NBS-19, NBS-20, and two in-house standards with analytical errors of <0.1‰ (1-σ) for $\delta^{13}C$ and <0.2‰ (1-σ) for $\delta^{18}O$.

Thin-Section Microscopy of Sediment and Rhizolith Samples

Polished thin sections of rhizoliths and paleosol sediments were made in order to determine the origin of the rhizolith carbonate (authigenic vs. diagenetic) and degree of pedogenesis. Thin section analyses were conducted using an Olympus SZX12 light microscope with attached digital camera at the William C. and Ruth Ann Dewel Microscopy Lab at Appalachian State University, and cathodoluminescence (CL) microscopy used a Reliotron cathodoluminescence microscope assembly, with voltage held at −8.0 kV, current 500 mA, and chamber vacuum held at 30–40 mTorr.

Bulk Geochemistry of Sediments

Bulk sediment samples were collected from each sedimentological unit identified in the trench excavation (approximately 500 mL of sediment was collected from the cleaned back wall of the trench exposure), including 100 mL subsampling of any identified paleosol units at 10 cm- or 50 cm-increments depending on the size and visible variation within each unit. Dr. Stan Mertzman at the X-ray Fluorescence Lab at Franklin and Marshall College analyzed paleosol subsamples, reporting major, minor, and trace element compositions (**Supplemental Data Table S1**). Major and minor elements were identified from powdered samples mixed with lithium tetraborate, placed in a platinum crucible, and heated until molten. The molten material was transferred to a platinum casting dish and quenched. The resulting glass disk was analyzed by X-ray fluorescence (XRF) and the results reported as weight percent of oxides (**Supplemental Data Table S1**). Trace element analysis involved mixing high purity copolywax powder with the crushed sample before pressing it into a pellet. Data are reported as parts per million (ppm) for trace elements. Working curves for each element were determined by analyzing geochemical rock standards (Abbey, 1983; Govindaraju, 1994).

Quantitative Climate Estimates Using Paleosol XRF Results and Paleosol Chroma

Mean annual temperature (MAT)

To calculate the degree of weathering within paleosol units, and ultimately mean annual temperature (MAT) of Loperot during the time of paleosol formation, we first applied the Paleosol Weathering Index developed by Sheldon et al. (2002) and Gallagher and Sheldon (2013):

$$PWI = [(4.20Na) + (1.66Mg) + (5.54K) + (2.05Ca)]^{*}100 \quad (1)$$

where Ca, Mg, Na, K, and Al are molecular weight of elements derived by converting the weight percent of oxides from XRF data into moles by dividing each oxide by its molecular mass (Sheldon and Tabor, 2009). We then used the PWI values to calculate the mean annual temperature using Equation 2 (Gallagher and Sheldon, 2013):

$$MAT = -2.74^{*}\ln(PWI) + 21.39(\text{Error} \pm 2.1^{\circ}C) \quad (2)$$

Per Lukens et al. (2017), calculation of MAT using PWI values is best suited for forested Inceptisols, Alfisols, and Ultisols. PWI values are known to decrease if paleosols are alkaline and/or poorly formed, which can produce calculated MAT values that are unrealistically low.

Mean annual precipitation (MAP)

To estimate mean annual precipitation (MAP), we calculated a value of hydrolysis for the paleosol units. The ratio of mobile cations to immobile cations within a soil profile can be a proxy for rainfall (e.g., Lukens et al., 2017). The reasoning behind this calculation is that high values of hydrolysis (>1) indicate an abundance of mobile cations in the soil, which implies aridity (i.e., mobile cations are still present within the soil and have not been leached by percolation). Values below 1 suggest high leaching of the soil, and thereby a high MAP.

We calculated the ratio of base elements to aluminum as a proxy for hydrolysis (i.e., weathering intensity; Retallack, 2001) using Equation 3:

$$\text{hydrolysis} = (Ca + Mg + Na + K)/Al \quad (3)$$

where Ca, Mg, Na, K, and Al are molecular weight of elements derived by converting the weight percent of oxides from XRF data into moles by dividing each oxide by its molecular mass (Sheldon and Tabor, 2009).

In order to quantify the degree of paleosol weathering, we then calculated the chemical index of alteration minus potassium (CIA-K; Sheldon et al., 2002):

$$CIA - K = (Al/(Al + Ca + Na))^{*}100 \quad (4)$$

where Al, Ca, and Na are molecular weight of elements derived by converting the weight percent of oxides from XRF data into moles by dividing each oxide by its molecular mass (Sheldon and Tabor, 2009). We then used the CIA-K value to quantify the mean annual precipitation per Sheldon et al. (2002):

$$MAP = 221.1e^{0.02(CIA-K)}(\text{Error} \pm 180\,\text{mm}) \quad (5)$$

Adams et al. (2011) recommend calculating MAP values in this manner on paleosols where the B-horizon is at least 1 m thick, so that both climate and time of pedogenesis may thoroughly

influence the soil geochemistry. They also recommend averaging the MAP calculations of several samples taken from the upper 50 cm of a B-horizon.

To corroborate calculated MAP values, we also tracked soil chroma upsection. Matrix soil color was determined using the method of Retallack (1990) using a Munsell Soil Color Chart (Munsell Color, 2010). Low soil matrix chroma values correspond to seasonal saturation, and higher chroma values tend to indicate aridity (Adams et al., 2011).

RESULTS (SITE LPM4)

Age of the Site

Various lines of evidence (radioisotopic, faunal, and geologic) indicate that the sediment exposed at Loperot is of early Miocene age. Whole rock $^{40}Ar/^{39}Ar$ analysis of two basalt samples obtained from a flow that directly overlies the ∼28 m of strata exposed at Loperot yielded ages of 16.96 ± 0.06 Ma and 17.10 ± 0.09 Ma (**Figure 4**), providing a minimum age for the sediment and fossils discussed herein (Liutkus-Pierce et al., 2017; **Supplemental Data Table S2**).

Comparisons of the fossil assemblage from Loperot with those from other sites indicate that this site is most similar to the Hiwegi Formation of Rusinga Island (Grossman et al., 2014), which is 18 Ma or older (Peppe et al., 2011). Loperot shares a unique proboscidean exclusively with Songhor (KNM-LP 53749: cf. *Archaeobelodon*; Grossman et al., 2014), a site dated to 19–20 Ma (Bishop et al., 1969; Hill et al., 2013), and we therefore assert that the fossil assemblage from Loperot supports the early Miocene age provided by the radiometric dates.

Fossil-bearing units at LpM4 (**Figure 3**) are composed of arkosic sandstones with little volcaniclastic input. Morley et al. (1999b) indicated that sediments exposed at Loperot belong to the Auwerwer Sandstone Formation (middle Miocene). However, consistent with the half-graben geometry and westward dipping units of the Lokichar Basin, the outcrops should become progressively younger westward toward the border fault and older to the east toward the Lokone Horst (**Figures 1B**, **2A**). Therefore, the Auwerwer Sandstone Formation and younger sediments would be exposed far to the west of the Lokone Horst, and older sediments of the Lokone Formation (consisting of sandstones nearest the flexural margin of the basin, and lacustrine shale further west toward the border fault) should outcrop nearest the flexural margin (the Lokone Horst). Several small westward-dipping normal faults disrupt the stratigraphy between the Lokone Horst and the Lokichar Fault (**Figure 2A**), but the site locations reported here occur just west of the Lokone Horst and are in the easternmost portion of the basin nearest the flexural margin, where normal faulting and tilting has more likely exposed the uppermost part of the Lokone Formation (**Figure 2A**). We therefore assert that, based on basin geometry and site location, the outcrops presented herein are part of the Lokone Formation (not the Auwerwer Sandstone Formation, per Morley et al., 1999b), consistent with the early Miocene age supported by our radioisotopic date and faunal analysis.

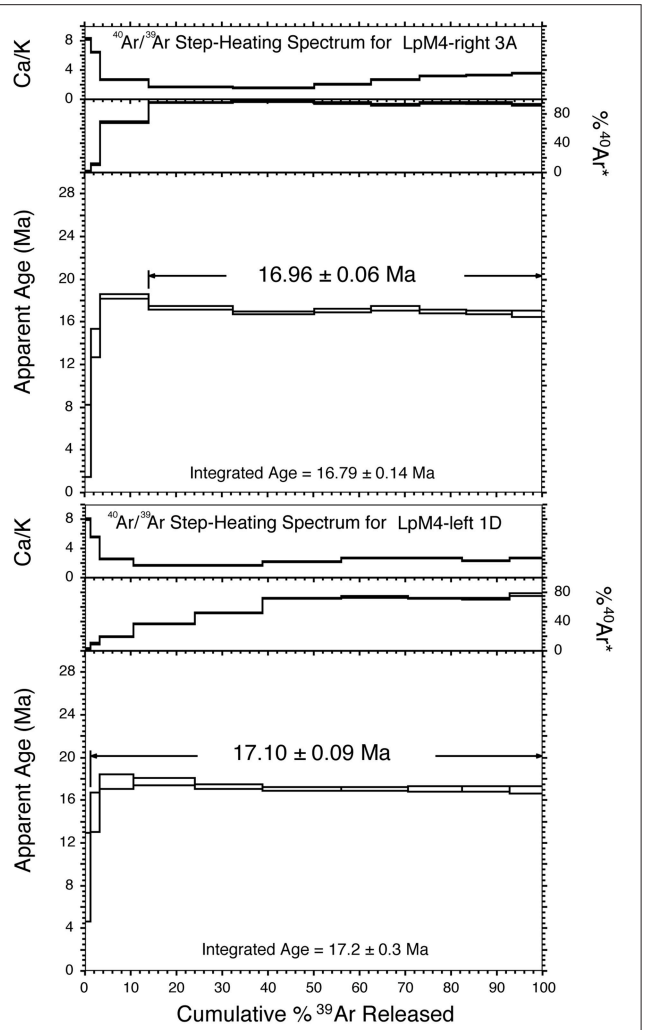

FIGURE 4 | $^{40}Ar/^{39}Ar$ incremental-heating spectra for samples LpM4-right 3A (**top**) and LpM4-left 1D (**bottom**). Reported $^{40}Ar/^{39}Ar$ dates are weighted age determinations and errors at the 2-σ confidence level. Both analyzed samples produced well-constrained plateau ages, which are statistically indistinguishable from each other. Plateau steps are indicated by lines ending in arrows.

Fauna

The fossils from Loperot include invertebrate and vertebrate remains (see Grossman et al., 2014 for a full list of vertebrate fauna). The invertebrate fossils include a bivalve (cf. *Coelatura*) and gastropods, including *Limicolaria* sp. (an achatinid land snail) and *Lanistes* sp. (an ampullariid that buries itself in mud during periods of drought; Van Damme, personal communication; **Figures 5A,B**). Vertebrate remains include fish, turtles and crocodiles, as well as numerous large and small mammals (Grossman et al., 2014). The catarrhine assemblage of Loperot is currently being described but contains both cercopithecoid and non-cercopithecoid catarrhines. In addition, Loperot has several mammals, including the oldest record in Africa of a shovel-tusked proboscidean (the amebelodontid *Platybelodon* sp.), a rhinoceros (*Chilotheridium pattersoni*), and a ziphiid whale (Wichura et al., 2015). Aquatic species such as the

FIGURE 5 | (A,B) Fossil invertebrates found at Loperot: an unionid bivalve (cf. *Coelatura*; **A**); an aestivating ampullariid (*Lanistes* sp.; **B**). **(C)** Medium- to coarse-grained, crossbedded sandstones that show thin (∼10 cm) fining upward sequences. Boundary between the crossbedded sandstone and red/gray siltstones beneath is erosional. Scale card is 8 cm wide.

beaked whale, crocodilians, and fish clearly indicate the presence of freshwater.

Typically, a mammalian community of forests includes relatively high proportions of medium to small arboreal frugivores and omnivores, and a smaller proportion of terrestrial herbivores (Reed, 1997). However, the assemblage at Loperot includes few arboreal or frugivorous taxa and is dominated by terrestrial herbivores (Grossman et al., 2014). Whereas this assemblage is small (about 20 species), it has a representation of mammals of different sizes, from small to large. Many of the taxa found at Loperot are also found at Rusinga Island and some at Songhor and Napak, all of which are reconstructed as forests (Grossman et al., 2014).

Sedimentology and Facies Description

At LpM4 (**Figure 1B**), we were able to identify the location where Meave Leakey and her team found monkey remains during previous excavations. The facies surrounding the fossil-bearing sediments at LpM4 is similar to sites LpM2 and LpM3, though we mainly report in detail the facies analysis from LpM4 because of the lack of exposure from sites LpM2 and LpM3. Nonetheless, the fossils are concentrated in medium- to coarse-grained cross-bedded sandstone units (**Figure 5C**) that exhibit thin fining-upward sequences, overlain by red silty claystone units with ped structures, rhizoliths, and gypsum rosettes (locally).

Fossiliferous Sandstone

This facies is characterized by brown (10YR 4/3) to light yellowish brown (2.5YR 6/3) poorly sorted, medium- to coarse-grained sandstone that contains bone fragments and, locally (LpM3), pumice pebbles, and cobbles. Minerals identified by optical microscopy include quartz, hornblende, and mica (with analcime as a likely secondary mineral). Where present, climbing ripples (LpM3) as well as planar and trough cross-bedding (LpM3, LpM4) indicate localized flow direction. At LpM4, individual sandstone units contain thin fining-up sequences (5–10 cm thick) along with scour-and-fill features (**Figure 5C**). Channel scours are several meters across and are capped with trough cross-stratified, coarse-grained sandstone (∼0.5 m-wide troughs).

Clay mineral content is extremely low compared to other facies (**Figure 6**). X-ray diffraction (XRD) analysis of the clay fraction yields broad based, low intensity peaks at low two-theta angles, but includes a 14.7 Å peak that expands to 17.3 Å upon

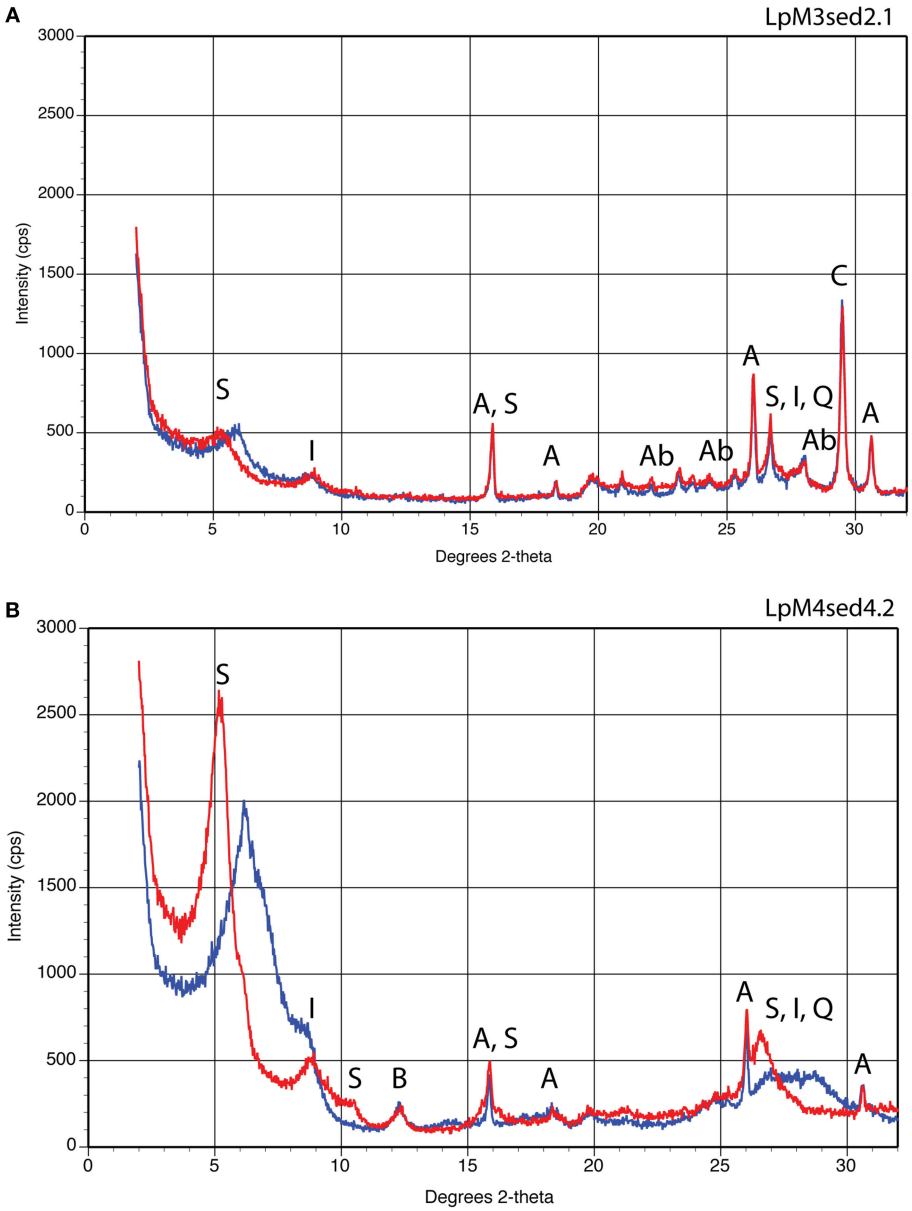

FIGURE 6 | X-ray diffraction results for sandstone **(A)** and silty claystone **(B)** facies. Blue line shows results under natural, air-dried conditions; red line shows results after 24 h exposure to ethylene glycol. **(A)** Sample of sandstone from site LpM3. Peaks correspond to smectite (S), illite (I), analcime (A), albite (Ab), quartz (Q), and calcite (C). **(B)** Sample of silty claystone from site LpM4. Peaks correspond to smectite (S), illite (I), beidellite? (B), analcime (A), and quartz (Q).

glycolation. XRD confirms the presence of dioctahedral smectite, illite, analcime, quartz, albite, and calcite; the smectite and illite are discrete phases and are not interstratified (**Figure 6A**).

Silty Sandstone/Siltstone

At each of the three localities, reddish brown (2.5YR 4/4) to red (10R 5/6) silty sandstone and/or siltstone units lie above the fossiliferous sandstone facies (**Figure 7A**). Sand/silt/clay ratios are approximately 60:30:10. This facies has a granular ped structure (ped size ranges from fine to very coarse, depending on site location), are calcareous, and locally contain rhizoliths, carbonate nodules (some up to 10 cm in diameter), and gypsum crystals (abundant at LpM4) (**Figure 7A**). The presence of granular peds, rhizoliths, gypsum crystals (and, in places, heavy gypsum cement), root traces, and plant macrofossils in this facies indicate that they are paleosols. Krotovina-like structures (**Figure 7B**) are abundant at LpM3 at the boundary between a red paleosol (below) and a very coarse, fossiliferous sandstone (above), and were likely formed by washing the overlying sand into cracks on the surface of the paleosol. Where the fossiliferous sandstone facies overlies this facies, the boundary is sharp (<2 cm) and indicates erosion. Microscopic

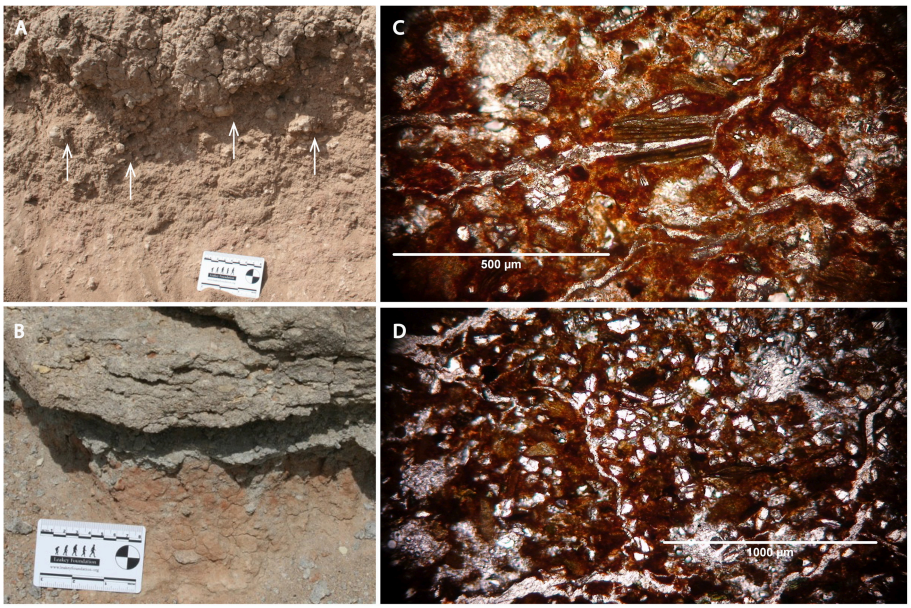

FIGURE 7 | Features of the silty claystone facies, including carbonate nodules (shown by arrows in **A**) and Krotovina-like structures **(B)**. Thin root traces **(C)** and plant microfossils **(D)** are abundant in thin section (plane light).

root traces and plant microfossils are abundant throughout (**Figures 7C,D**).

Optical and thin-section microscopy identified detrital quartz, hornblende, and biotite, along with gypsum and analcime that were likely deposited as secondary (post-depositional) minerals. XRD analysis of the clay fraction showed well-formed peaks in low two-theta angles that expanded upon glycolation, confirming the presence of dioctahedral smectite as well as illite, analcime, quartz, and possible beidellite. The smectite and illite are not interstratified (**Figure 6B**).

Stratigraphy

All units in the region dip shallowly (∼5°) to the W/SW. A columnar basalt unit caps the stratigraphic section and can be traced for several kilometers. We identified 30 stratigraphic units exposed in the ∼28 m-thick step-trench excavated at LpM4 (**Figure 8**). A coarse sandstone unit found near the top of the section (Unit 3) exhibits well-defined trough and planar cross-lamination that indicates flow to the north. Unit 11 also exhibits cross-laminations with foresets that dip northward. Unit 28, near the base of the section, is a heavily indurated medium sandstone with abundant planar cross-lamination, although flow direction alternates between east and west. This resistant unit is recognizable throughout LpM4 and was termed the "ledge sand" (**Figure 8**).

Within the 28 m-thick section exposed in the trench, we identified 11 meter-scale fining-upward cycles (**Figure 8**). Each cycle begins with a sharp erosional basal contact between an underlying paleosol and the overlying sandstone unit. The thickness of the sandstone unit varies, as does the thickness of the fining-upward cycle. Cycles fine upward gradually from coarse sandstone to silty sandstone or siltstone (e.g., Unit 28–Unit 26; **Figure 8**), but some cycles contain abrupt contacts between a basal sandstone and the siltstone at the top (e.g., Unit 23–Unit 22; **Figure 8**).

Additional LpM4 stratigraphic sections (Exposure 1 and Exposure 2) were measured and described from outcrop exposure, but were not trenched (**Figure 3**). Correlating the stratigraphic sections around site LpM4 proved to be challenging and indicates some regional heterogeneity of facies. For example, the "ledge sand" (Unit 28) in the trench appears to correlate to two sandstone units at an exposure only 0.5 km to the northeast. Despite such heterogeneity, each stratigraphic section exhibits the fining-upward cycles identified within the trench (**Figure 8**).

Rhizolith Size Variation, Petrography, and Isotope Geochemistry

Rhizoliths were identified in the trench (Unit 13) and in Exposure 1; those in Exposure 1 were assigned to Units 17, 22, and 26 within the trench based on best estimates of stratigraphic correlation. Only 2 rhizoliths were found in Unit 13, located ∼90 cm below the surface of the unit. Rhizoliths in other units were significantly more abundant and found associated with carbonate nodules.

We analyzed the size variation and stable isotopic signatures of rhizoliths from Unit 17, Unit 22, and Unit 26 (**Figure 9**). Comparison of rhizolith widths collected from each layer indicates distinct average widths (**Figure 9A**): 5.2 mm for Unit 17 ($n = 58$), 7.9 mm for Unit 22 ($n = 56$), and 10.2 mm for Unit 26 samples ($n = 33$). The range in widths for Unit 26 samples is higher (st. dev. = 3.8 mm) than for Unit 17 (st. dev.

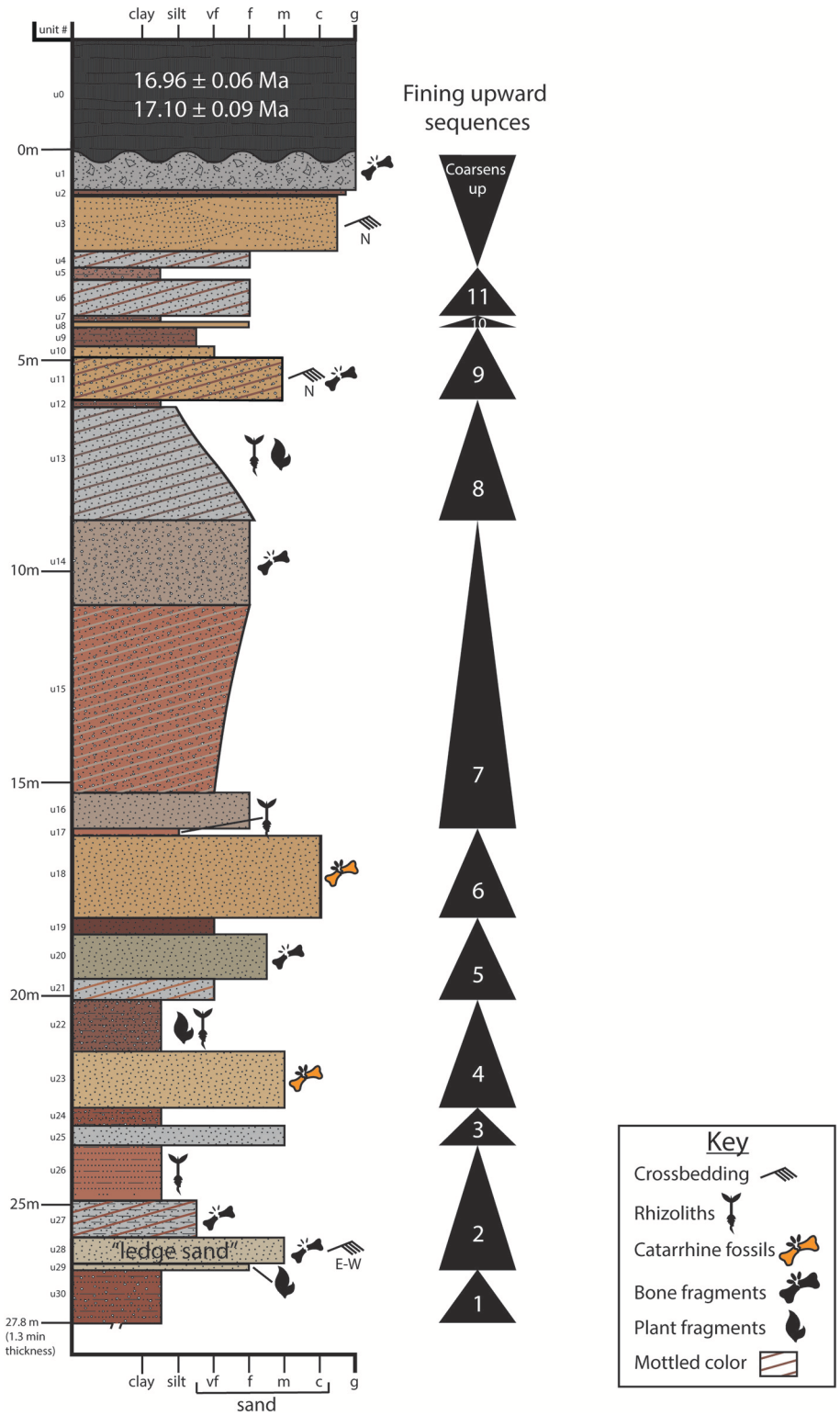

FIGURE 8 | Sedimentological description of the 28 m trench excavated at site LpM4 in 2016 (trench excavation location noted on **Figure 3**). Eleven fining-upward cycles are identified, along with the presence of key sedimentary structures and fossils. Highly fossiliferous units (18, 23, and 27) sit well below the basalt (Unit 0) dated to ∼17 Ma. Catarrhine fossils were found in stratigraphic levels correlated to Units 18 and 23.

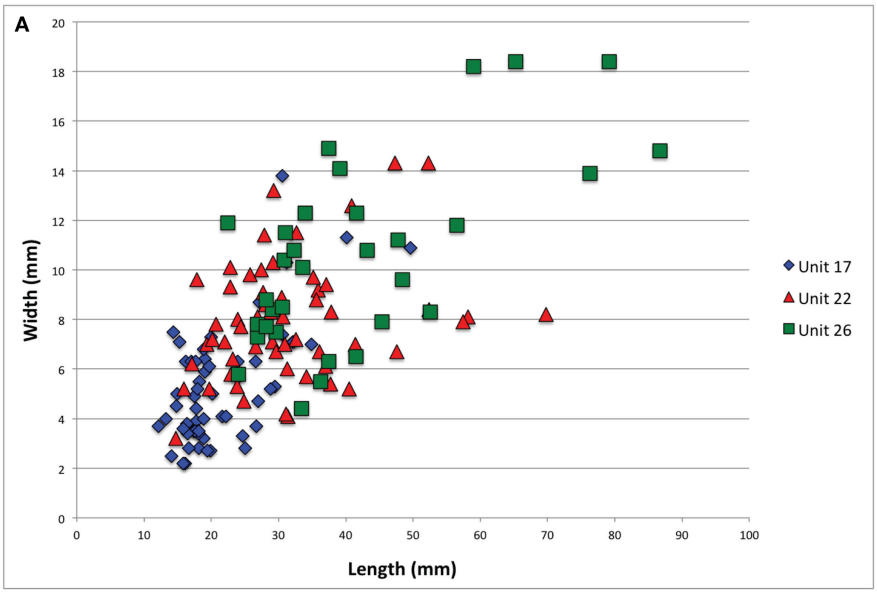

FIGURE 9 | Size and stable isotopic composition data from rhizoliths. **(A)** Size variation (width vs. length) of rhizoliths collected from Units 17, 22, and 26, immediately overlying rich fossil-bearing strata from LpM4. **(B)** Comparison of $\delta^{18}O$ and $\delta^{13}C$ values (‰, V-PDB) for rhizolith carbonate microsampled from above each fossil-bearing unit. The range in $\delta^{18}O$ values is similar for samples from all three units, however the average $\delta^{13}C$ value for Unit 22 unit is significantly higher than that in Units 17 and 26.

= 2.4 mm) and Unit 22 (st. dev. = 2.4 mm) samples, as is the average rhizolith width.

Petrography of Rhizoliths

Optical and cathodoluminescence (CL) microscopy confirm that the rhizoliths are micritic to microsparitic calcite and have a uniform to patchy luminescence that is bright yellow to orange (**Figure 10A**), consistent with minimal diagenetic alteration (Cerling, 1991). Alpha fabrics identified include complex desiccation cracks infilled by equant sparry calcite (**Figure 10B**) and corona grain coatings on detrital grains (e.g., quartz, hornblende; **Figure 10B**; Wright, 1990). Rhizolith calcite lacks characteristics of beta-fabrics, such as *Microcodium* grains, needle-fiber calcite, or alveolar-septal fabric (Wright, 1990). Organic material is included within the analyzed rhizoliths, but is too small to be identified to plant type. Based on the classification of Klappa (1980), these rhizoliths exhibit features typical of root casts that formed during or after the decay of the plant as the root or stem void infilled with sediment and was subsequently cemented.

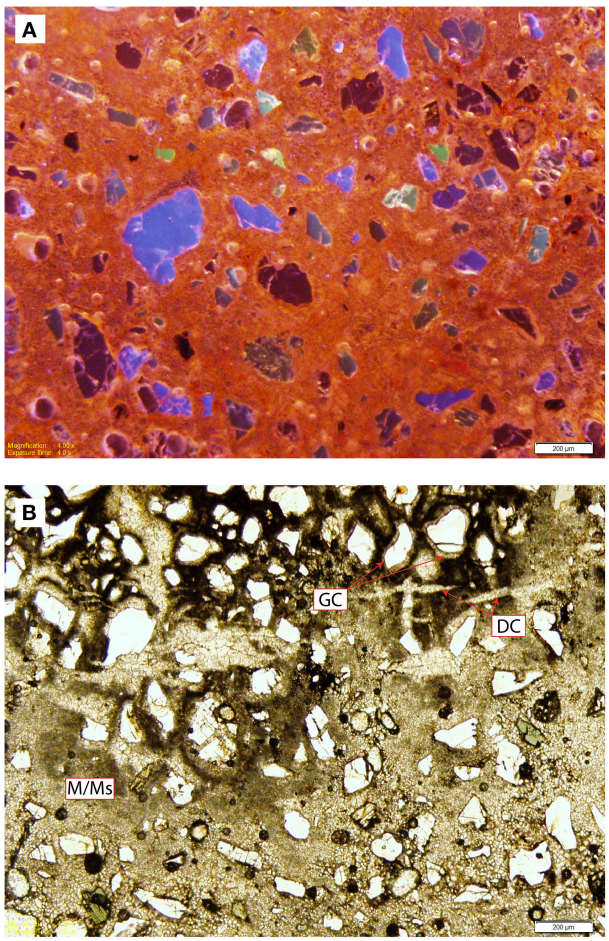

FIGURE 10 | Results of the thin section analysis of rhizoliths from LpM4. **(A)** Cathodoluminescence microscopy of a rhizolith from Unit 26, showing uniform to patchy luminescence. **(B)** Plane-polarized light microscope image of a rhizolith from Unit 26, showing micritic to microsparry calcite (M/Ms), complex desiccation cracks infilled with equant calcite crystals (DC), and radial grain coatings (GC).

Stable Isotopic Results

Stable carbon and oxygen isotope trends are routinely used to assess the degree of alteration (diagenesis) in carbonates, particularly when combined with petrographic and CL study. Because pedogenic carbonates typically precipitate from soil moisture (derived from meteoric water), traditional approaches using isotope cross plots to screen for meteoric alteration do not apply (cf. Banner and Hanson, 1990). Instead, we focus on using transmitted light and CL microscopy to characterize evidence for alteration by documenting variation in crystal size and luminescent patterns of rhizolith calcite.

Recrystallization of micritic calcite can be detected with ease using CL when secondary larger sparry calcite crystals crosscut primary micrite. Uniform luminescence of rhizolith calcite from Loperot is consistent with little to no diagenetic overprint (**Figure 10A**) and supports our interpretation of the stable isotopic composition as an accurate reflection of paleoenvironmental conditions.

Isotopic data (**Supplemental Data Table S3**) indicate that rhizoliths from the oldest (Unit 26) and youngest (Unit 17) layers have similar values (see **Figure 8** for stratigraphic positions and **Figure 9B**). Rhizoliths from these units have average $\delta^{13}C$ values of −10.5‰ (Unit 26) and −10.6‰ (Unit 17), and range in $\delta^{18}O$ values from −4.8‰ to −2.3‰ and −6.0‰ to −2.7‰, respectively. Unit 22, however, has a higher average $\delta^{13}C$ value (−8.2‰) and a larger range of $\delta^{18}O$ values (−7.0 to −1.8‰) compared to the other units (**Figure 9B**). The range in $\delta^{13}C$ values for Unit 22, however, is greater and the average value is higher.

Environmental Reconstruction

Raw and processed XRF data from bulk sediment samples from Loperot are compiled in a supplementary dataset and are keyed to the stratigraphic units presented in **Figure 8** (**Supplemental Data Table S1**).

Mean Annual Temperature (MAT)

Values of PWI for each analyzed paleosol unit range from 50 to 112 (**Supplemental Data Table S1**) and indicate MAT values ranging from 8.5 to 11°C, which are unrealistically cold for equatorial Kenya during the early Miocene. Hydrolysis values from the Loperot paleosols are all greater than 1, indicating alkaline soils. PWI values are known to decrease if paleosols are alkaline and/or poorly formed, which can produce calculated MAT values that are unrealistically low. We, therefore, infer that due to their alkalinity, the Loperot paleosols are not well suited for MAT calculations using the PWI method (Equation 2).

Degree of Weathering and Mean Annual Precipitation (MAP)

Base loss ratios (i.e., the abundance of a mobile base cation compared to the abundance of a relatively immobile cation like Ti) indicate little mobility of cations and hydrolysis values (Equation 3) above 1 indicate high soil alkalinity and minor leaching of the Loperot sediments, which suggests a semi-arid to arid climate. Extremely low (<0.2) values of Al/Si (a measure of clayeyness) also indicate little hydrolysis, which should produce Al concurrent with clay production (Retallack, 1990).

Admittedly, the Loperot paleosols may not be ideal candidates for MAP calculation using CIA-K, as Adams et al. (2011) warn that this method is best applied to paleosols containing <5% bulk carbonate and no carbonate nodules. Several of the Loperot paleosols did exhibit significant carbonate cement and the presence of carbonate nodules; however, we attempted this method on the paleosol found in Unit 13, which exhibited low carbonate cement, no nodules, and was 2.5 m thick. CIA-K values for Unit 13 ranged from ∼37 (at 0.5 m) to ∼60 (at >1.5 m) (**Supplemental Data Table S1**). Taking these suggestions, we used CIA-K values for Unit 13 from 0.5 m and 1.0 m depth (within the upper B-horizon), and calculated MAP values ranging from 462 to 545 mm/year (average = 503 mm/yr ± 180 mm) (**Supplemental Data Table S1**), indicating a semiarid (250–500 mm/yr) to subhumid (500–1000 mm/yr) environment (Bull, 1991; Lukens et al., 2017). We realize that this may not be an estimate of MAP over the entire period of sediment deposition

TABLE 1 | Soil chroma values and environmental indication for paleosol units exposed in the trench at LpM4.

Unit #	Munsell chroma	Indication
5	3	Semi-dry
7	3	Semi-humid
9	3	Semi-humid
12	3	Semi-humid
13	3	Semi-humid
15	4	Semi-dry
17	6	Dry
19	4	Semi-dry
22	5	Dry
24	6	Dry
26	6	Dry
30	6	Dry

at site LpM4, and we also recognize that while Unit 13 did not contain any carbonate nodules, it did contain a few rhizoliths at a depth of 90 cm.

To further investigate MAP values, we also tracked soil chroma upsection (Munsell Color, 2010; **Table 1**). Low soil matrix chroma values correspond to seasonal saturation, and higher chroma values tend to indicate aridity (Adams et al., 2011). **Table 1** shows the dominant soil matrix chroma values for paleosols within the trench excavation at LpM4; we report an overall decrease in soil chroma upsection.

DISCUSSION

Early Miocene Critical Zone Reconstruction From Loperot

Detailed stratigraphic analysis of the exposures at Loperot indicates that the catarrhine fossils found in 2012 did not come from the same stratigraphic unit (a mandible was found in Unit 23, and a molar was found in Unit 18) (**Figure 8**). This begs the question whether Loperot's catarrhines inhabited a similar habitat at different times or whether they inhabited the site continuously even under different environmental conditions. We, therefore, use a multi-proxy approach to reconstruct the Critical Zone of Loperot (Nordt and Driese, 2013). The strata are laterally extensive and are capped by a layer of datable basalt, making Loperot an ideal location to place early Miocene primate fossils in spatial, temporal, and paleoenvironmental context. This study, therefore, is the first to apply the Deep Time Critical Zone concept to the stratigraphy at Loperot in order to interpret the lithologic, atmospheric, biologic, and hydrologic conditions of this area during the early Miocene (Nordt and Driese, 2013).

Lithosphere

The sand-dominated facies identified at Loperot represents sediments deposited in fluvial channels, and the siltstone facies represents ancient soils that developed along the river's floodplain. The recurrent shift in facies (the fining-up cycles) from fluvial sandstone to silt-dominated paleosols suggest that there was a sustained, localized change in the depositional environment over time that we attribute to river meander and/or river avulsion (Hajek and Edmonds, 2014). Stratigraphic correlation across distances greater than ∼50 m indicates facies heterogeneity, suggesting a large river system composed of a main trunk stream along with numerous smaller (ephemeral?) channels that produced a rapidly changing landscape as the river and its tributaries meandered and avulsed [**Figure 8**; Hajek and Edmonds, 2014].

The paleosols above the fossil-bearing layers contain rhizoliths, gypsum, plant microfossils, and land snails such as *Limicolaria* and *Lanistes* (both which tend to inhabit floodplains that experience seasonal flooding; Van Damme, personal communication). These paleosols indicate periods of stability on the land surface, long enough for the sediment (floodplain silts and fine sands) to alter to soils—possibly hundreds to a few thousands of years (Atchley et al., 2013).

The presence of smectite (formed from weathering of mafic volcanics) and analcime (a zeolite that forms from altered intermediate/mafic volcanic rocks) points to a volcaniclastic source, and illite indicates either alteration of K-feldspar and/or muscovite or recrystallization of smectite (Nadeau et al., 1985; Velde and Barré, 2009). Analcime and gypsum found in the paleosol units are most likely secondary (alteration) minerals that indicate deposition in an arid climate (Mack and James, 1994; Ashley et al., 2014; mean annual precipitation <250 mm/yr), however it is difficult to know at what point in the last 17 million years these secondary minerals formed in the Loperot sediments.

The granular ped structure (formed by wetting/drying), abundance of vertical rhizoliths, poor horizonation, and absence of vertic structures (such as gilgai micromorphology and intersecting slickensides) suggests that the Loperot paleosols are Fluvisols (FAO, 2001). Fluvisols typically form in arid to semiarid regions with highly seasonal precipitation near well-drained river channels, where vegetation taps a consistent source of groundwater (Wynn, 2000). The parent material is often well-sorted channel sand and floodplain silt and mud, and horizonation is poorly to weakly developed. *Limicolaria* snails found in the Loperot sediment support this interpretation of seasonally inundated floodplains (Pickford, 1995; Retallack et al., 2002).

Climate

Because paleosols are a product of weathering and environmental conditions (temperature and humidity), the bulk geochemistry of paleosols can provide information about the conditions under which they formed (i.e., the degree of weathering, the mean annual precipitation under which the soils formed, and (indirectly) the mean annual temperature of soil formation) (Retallack, 2001).

Mean annual temperature

Calculated mean annual temperature values (using PWI) indicate a range from 8.5° to 11°C (**Supplemental Data Table S1**). Such cool temperatures are unrealistic for equatorial Africa in the early

Miocene, and we attribute this anomalous result to the alkalinity of the paleosols producing low PWI values.

Pedogenic carbonates often precipitate in equilibrium with soil water and their $\delta^{18}O$ values are a function of the temperature at which the carbonate precipitates and the $\delta^{18}O$ of the soil water (Craig, 1965; Passey, 2012). Soil water is often derived from local meteoric water, but without a constraint on the $\delta^{18}O$ of Miocene precipitation at Loperot or an understanding of the processes that may have affected the soil water $\delta^{18}O$ values (i.e., soil water may have a more positive $\delta^{18}O$ value than meteoric water due to evaporative concentration), it is inappropriate to use the $\delta^{18}O$ values of the Loperot rhizoliths to reconstruct precipitation temperature. Passey (2012) explains well the many factors that affect temporal variation of soil temperature at depth, including thermal conductivity and diffusivity of the soil, thermal transport via rainwater seepage, etc. To further complicate the matter, pedogenic carbonates in temperate climates tend to form during (and therefore record) warm season conditions, whereas carbonates that form in tropical climates record mean annual temperature. More concrete inferences regarding mean annual temperature (or warm season temperatures) will be addressed by future clumped isotope thermometry.

Mean annual precipitation

The presence of carbonate rhizoliths in several stratigraphic units supports the interpretation of a semiarid to dry subhumid climate with pronounced seasonality where evapotranspiration exceeds precipitation (Adams et al., 2011), and suggests the presence of moderately drained soils (Kraus and Hasiotis, 2006). Soil chroma values (**Table 1**) for the lower portion of the trench (Units 15 to 30) range from 4 to 6 and indicate arid to semiarid conditions. Units 12, 9, and 7 had chroma values of 3 and suggest a more subhumid climate. Unit 13 values for CIA-K (from 0.5 m and 1.0 m depth, within the upper B-horizon) produced calculated MAP values ranging from 462 to 545 mm/year (average = 503 mm/yr $\pm$ 180 mm) (**Supplemental Data Table S1**), indicating a semiarid (250–500 mm/yr) to subhumid (500–1000 mm/yr) environment (Bull, 1991; Lukens et al., 2017).

Hydrosphere

The presence of aquatic species, such as crocodiles, fish, bivalves, and a whale (Mead, 1975; Wichura et al., 2015), coupled with sedimentary structures such as cross-bedding, climbing ripples, and fining-upward sequences of the sandstone units, indicate fluvial deposition in a large, freshwater river system. However, there is variability in the flow regime preserved in the facies. The presence of bivalves, turtles, crocodiles, and a whale indicates a large, low-gradient, perennial river that drained eastward toward the Lamu Embayment and the Indian Ocean, providing a fluvial conduit for the whale found at Loperot (Wichura et al., 2015). However, the thin fining-upward sequences within the sandstone units at LpM4 suggest that, at least locally, flow was shallow with coarse bedload. The presence of albite and the coarse, poorly sorted sandstone facies indicates immature sediment that was likely close to a volcaniclastic source (also supported by the presence of pumice pebbles and volcanic rock fragments at LpM3).

The eleven fining upward cycles identified within the 28 m-section at LpM4 indicate that this region was dynamic and rapidly changing during the early Miocene, however it is difficult to know, based solely on the sedimentology, whether the fining-upward cycles are due to climate change (e.g., as climate dries, the river ceases to flow) or are autocyclic (e.g., progradational channel avulsion; Hajek and Edmonds, 2014). The isotopic results seem to suggest that climate (i.e., evaporation/precipitation ratios indicated by $\delta^{18}O$ values of rhizoliths) did not change dramatically upsection (values for every unit measured remain within a range from ∼-6.0 to −2.0‰), and therefore the short-term shifts in the river's course (recorded by the fining upward cycles) are unlikely due to climate change.

At the top of the stratigraphic section, the fining-up cycles change to a single coarsening-up sequence that is then capped by a columnar basalt unit, indicating extrusive volcanism. We therefore propose that, superimposed on the short-term shifts in the river's course indicated by the fining upward cycles, there was a larger-scale change in the overall direction of river flow, indicated by the change in dip direction of the foresets of crossbeds upsection from east-west (Unit 28) to north (Units 11 and 3), that was most likely due to a shift in regional tectonics. It is possible, though difficult to determine at this time, that this regional tectonic activity was the cause for the lava flow which caps the Loperot stratigraphy.

Biosphere (Flora)

Because the length of the rhizoliths collected from each unit is likely an under-estimate of its original length (i.e., they could be broken *in situ* or during collection, thus not necessarily representative of the original root length), we instead focus on the importance of the varying widths of the rhizoliths from each unit. The overall width and variability of widths of rhizoliths is greater in Unit 26 ($1\sigma = 3.8$ mm, $n = 33$) compared to Units 17 and 22 ($1\ \sigma = 2.4$ mm for both, $n = 58$ and $n = 56$ respectively). This may indicate either a greater variety of plant types on the surface during deposition of Unit 26, or that plants in that unit had a longer amount of time to grow and rhizoliths preserve plant roots at various stages of development (young and old). It is unlikely that the range is due only to variation in plant type, since $\delta^{13}C$ values of Unit 26 rhizoliths differ by only ∼1‰ (−11.2 to −10.1‰, C_3 plants).

The isotopic composition of soil CO_2 is essentially constant below ∼20 cm depth, and as such, the composition of pedogenic carbonate formed at these depths would record the $\delta^{13}C$ value of the soil-respired CO_2 of the local biomass (Cerling, 1991; Passey, 2012). Therefore, in order to reconstruct paleovegetation using the $\delta^{13}C$ value of soil carbonates as a proxy for local biomass the depth of the carbonate samples within the paleosol is important—samples that formed in the upper 10–20 cm may record a $\delta^{13}C$ value influenced by atmospheric CO_2 rather than a true representation of soil-respired CO_2 (Cerling, 1991; Passey, 2012). We interpret the rhizoliths collected from the

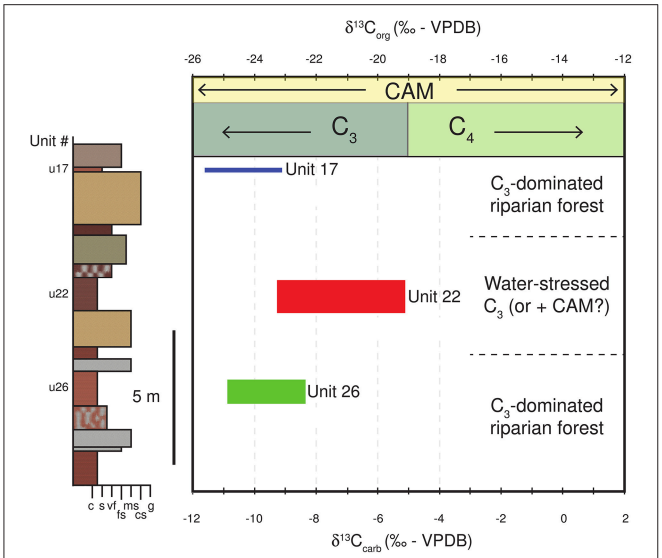

FIGURE 11 | Range in $\delta^{13}C$ values measured from rhizoliths in Units 26, 22, and 17, shown in stratigraphic position next to the lower part of the stratigraphic column of the trench (units 16–30), and compared to the known ranges of carbon isotopic composition of plant biomass (C_3, C_4, and CAM plants). Data indicate that the paleoenvironment at Loperot changed from a purely C_3 riparian woodland (Unit 26), to a water-stressed C_3- (or arid-adapted CAM-plant) dominated environment (Unit 22), and back to C_3 riparian woodland (Unit 17).

trench and Exposure 1 at LpM4 as primary pedogenic carbonate because they are (a) found within units showing evidence of pedogenesis (e.g., exhibiting ped structure), (b) found in association with abundant carbonate nodules (which we interpret to have formed within a Bk horizon), and (c) micritic and not sparry (and thus have not experienced diagenesis)(Passey, 2012). This is consistent with rhizoliths found *in situ* in Unit 13 at depths of 90 cm. We envision that the Loperot rhizoliths formed in the manner described by Klappa (1980), where sediment and/or cement infills a root mold or tubule after the plant root has died.

During the early Miocene the isotopic composition of soil-respired CO_2 and the resulting pedogenic carbonate is dominated by C_3 biomass (Cerling, 1991). The range in rhizolith $\delta^{13}C$ values for Units 26 and 17 are consistent with previous reports of paleosol carbonates from the early Miocene in East Africa (−10 to −12‰; Cerling, 1991) and represent periods of time when the contribution of C_4 biomass to the soil was insignificant; values plot within the "pure C_3/forest or woodland" category of (Wynn, 2000) **Figure 11**) when adjusted for slightly more positive early Miocene atmospheric $\delta^{13}C$ values (−6.0‰; Tipple et al., 2010).

The shift to more positive average $\delta^{13}C$ values of Unit 22 rhizoliths could be explained either by a biological or environmental cause, or some combination of both. For example, the more positive $\delta^{13}C$ values of rhizoliths from Unit 22 could be explained by a change in vegetation type. In order for the average $\delta^{13}C$ value to increase from −10.1 to −8.2‰, it would require a contribution of ∼25% C_4 biomass into the ecosystem at that time, assuming atmospheric CO_2 levels during the early Miocene were <700 ppmV (cf. Cerling, 1991; **Figure 11**), which appears to be true based on atmospheric CO_2 modeling estimates (e.g., Royer et al., 2014). This is unlikely considering that C_4 plants did not significantly contribute to soil biomass prior to 8 Ma during the late Miocene (Morgan et al., 1994; Urban et al., 2010). Additionally, (Retallack, 1990) indicates that grass roots have a mean diameter of <2 mm, which is significantly smaller than the mean width of Loperot rhizoliths (**Figure 9A**). In fact, the average width of the Unit 22 rhizoliths is not significantly different from those found in Unit 26, suggesting that a change in vegetation type does not explain the increase in $\delta^{13}C$ values in Unit 22.

Alternatively, several environmental factors can yield more positive $\delta^{13}C$ values, including lower temperature, high soil porosity, diagenetic alteration, and/or low plant respiration rates (Cerling, 1991). Low temperature can be ruled out because the range in $\delta^{18}O$ values for Unit 22 is nearly identical to the range for Units 17 and 26 (indicating little change in the temperature at which the calcite precipitated; **Figure 9**). The grain size of the Unit 22 soil matrix (siltstone) precludes high porosity as a viable explanation, and thin section analysis of the Unit 22 rhizoliths (micritic calcite) suggests that diagenesis was insignificant. Finally, low respiration rates are equally unlikely given the abundance of rhizoliths found within Unit 22 and their similar size and shape to rhizoliths from other units.

Instead, we suggest that the rhizoliths from Unit 22 represent similar vegetation (C_3) as in Unit 26 and Unit 17 but that the increase in $\delta^{13}C$ values is due to environmental stress. The discrimination against ^{13}C by C_3 plants is known to decrease under arid, high temperature, or low CO_2 conditions, which can lead to increased $\delta^{13}C$ values of biomass and, thus, soil-respired CO_2 (Farquhar et al., 1989; Passey, 2012). Passey (2012) reports that average $\delta^{13}C$ values of C_3 plants from arid regions (with mean annual precipitation < 200 mm/yr) can be as much as ∼5‰ more positive than C_3 plants in more humid ecosystems (mean annual precipitation > 1500 mm/yr), suggesting that in systems where the contribution of C_4 vegetation can be considered negligible (i.e., Loperot), the $\delta^{13}C$ value of pedogenic carbonates can be a proxy for paleoprecipitation (Kohn, 2010). An increase of $\delta^{13}C$ values from Unit 22 rhizoliths could indicate a change to more arid conditions, which incidentally coincides with a slight increase in the most positive $\delta^{18}O$ values reported within the rhizoliths from the same unit (**Figure 9B**).

Soil-respired CO_2 from CAM plants admittedly have a large range in $\delta^{13}C$ values of their biomass (from ∼-30‰ up to ∼11‰), but $\delta^{13}C$ values of CAM plant biomass from arid environments is more similar to C_4 plants, and $\delta^{13}C$ values of CAM plants from more humid environments are more similar to C_3 plants (Szarek and Troughton, 1976; Marshall et al., 2007). Thus, it may be possible that the slight increase in $\delta^{13}C$ values of rhizoliths from Unit 22 record a greater contribution of more arid-adapted CAM plants. Currently, we cannot rule out whether the increase in $\delta^{13}C$ values from Unit 22 records an increase in arid-adapted CAM plants or less ^{13}C discrimination by C_3 plants in the region due to environmental stress, but nevertheless a change to more arid conditions appears likely during the formation of Unit 22.

SYNTHESIS

Through our multi-proxy analysis of the stratigraphy and geochemistry of site LpM4, we infer that the deposition of the sediments in the lower section was under arid to semiarid conditions where the presence of a large perennial river provided water for a riparian forest. Given the overall dry climate indicated by the soil chroma and the lack of forest-dwelling fauna, it is likely that conditions became significantly more open and shrubby with increased distance away from the river's edge and that numerous ephemeral tributaries fed the larger perennial river. Riparian forest conditions prevailed during formation of Unit 26, with trees and shrubs abundant near the banks of the river system that flowed from west to east. As the river and its tributaries meandered, crossbedded sandstones were deposited and Fluvisols formed on the floodplains under pronounced seasonality (as indicated by the presence of rhizoliths and the mollusk species). Afterward, climate dried (as indicated by the slight increase in Unit 22 $\delta^{18}O$ values) and the landscape became dominated by water-stressed C_3 plants (possibly including arid-adapted CAM plants) during the formation of Unit 22. Subsequently, more negative $\delta^{13}C$ values indicate that the riparian forest once again dominated the landscape while Unit 17 formed. During deposition of Units 13 to 1, soil chroma values decreased indicating that climate began to shift from arid to semiarid to subhumid. At that time, the main direction of river flow shifted to the north, as indicated by a change in the dip direction of crossbed foresets in Unit 3 before a volcanic event covered the region in a thick basalt flow ∼17 million years ago.

CONCLUSIONS

In general, there is a large body of work that suggests forests and woodlands were widespread across equatorial Africa during the Oligocene-Miocene transition and continued until the late Miocene (e.g., Andrews and Van Couvering, 1975; Uno et al., 2016). Accordingly, many reconstructions of the Oligocene-Miocene climate suggest an overall warm, humid (>1,000 mm/yr) regime prior to 16.8 Ma (Talbot et al., 2004; Couvreur et al., 2008). However, recent studies are demonstrating that regional climates and local conditions preserve a more nuanced picture. Retallack et al. (2002) reported a more modest mean annual precipitation for the region of southwestern Kenya during the early Miocene, ranging from ∼400 to 750 mm/yr. Evaporites (e.g., halite hoppers) reported in the Grit Member of the Hiwegi Formation at Rusinga Island (∼18 Ma) indicate a short arid interval in what was a primarily a mosaic of seasonal forests and woodlands near a river for most of that time (Maxbauer et al., 2013). At Karungu, not far from Rusinga, conditions were quite dry and arid at least during one stratigraphic interval (NG15) during the early Miocene (Driese et al., 2016). This resulted in a fauna with very few primates, although taxonomically they do not differ from those found in much greater abundance at Rusinga (Lukens et al., 2017). As continental rifting began in Kenya, forests began to shrink due to decreased rainfall and increased seasonality, becoming more isolated wooded ecosystems (Vincens et al., 2006). At sites to the north of, but of similar age to, Loperot, Vincens et al. (2006) reported abundant fern pollen, indicating that these regions were still covered by rainforests during the early Miocene. However, the geochemical proxies and $\delta^{13}C$ data reported here indicate that, at least at times, Loperot experienced a semiarid climate and shifted from a riparian forest/woodland to a more arid, open habitat. This may indicate that, by the early Miocene, Loperot had started to transition to a more open habitat with more isolated forests and a semiarid precipitation regime, whereas sites to the north were still humid.

Our results do not support the hypothesis of an extensive, humid, multistoried closed-canopy forest at Loperot during the early Miocene, similar to that suggested for some other sites preserving non-cercopithecoid catarrhine fossils (i.e., Rusinga and Songhor). Instead, our analyses indicate a dynamic and changing paleoenvironment at Loperot, with a semiarid riparian forest (where trees concentrated near the banks of a large, perennial river) that shifted to a more open environment as climate changed and/or the river meandered away. This interpretation is consistent with a growing body of evidence that African climate and associated environments experienced strong regional effects and that arid regions clearly existed by the early Miocene. Much of the work reconstructing early Neogene environmental conditions in Africa was driven by questions about faunas associated with early ancestors of apes and humans. Exploring sites where the catarrhine assemblage is dominated by cercopithecoids, or alternatively where cercopithecoids are absent, may provide important information about how environmental factors affected catarrhine evolution.

AUTHOR CONTRIBUTIONS

AG, CL-P, and FK designed the study and CL-P wrote the manuscript. CL-P, KT-B, AG, and FK conducted the fieldwork. CL-P and KT-B completed all geological excavations and AG and FK completed the paleontological excavations and analyses. CL-P, KT-B, LB, and OB completed the sedimentological lab analyses. SM and SH completed the radioisotopic dating of the basalt samples. CL-P, CE, and JW contributed to the discussion and interpretation of the stable isotopic results.

ACKNOWLEDGMENTS

The authors wish to gratefully acknowledge funding for this project provided by the Leakey Foundation (2011) and various agencies at Appalachian State University (Office of Student Research, Cratis D. Williams Graduate School, the Deans Office of the College of Arts and Sciences, and the Office of Research and Sponsored Programs to CL-P). We are grateful to the Kenyan government, the National Museums of Kenya (NMK), and Dr. Frederick Kyalo Manthi for their continued dedication to ongoing research at Loperot, including permits and research association. Benson Kyongo, Longoria Eyanae,

Leonard Kyalo, John Dunda, Tonny Moru, Johnmark Ekeno, Martin Lele, and the people of Loperot are sincerely thanked for their assistance in the field. Tanzhuo Liu is thanked for his work analyzing and distilling the radioisotopic data from the basalt samples. The ideas presented here have developed and improved significantly due to discussions with Dirk Van Damme, Michelle Goman, Lawrence Kiage, Dan Deocampo, Scott Marshall, Steve Driese, Brian Zimmer, Guichuan Hou, Anthony Love, Rodderick McGarva, and Oscar Armengolt and we wish to thank them sincerely.

SUPPLEMENTARY MATERIAL

The Supplementary Material for this article can be found online at: https://www.frontiersin.org/articles/10.3389/fevo.2019.00044/full#supplementary-material

REFERENCES

Abbey, S. (1983). *Studies in "Standard Samples" of Silicate Rocks and Minerals* 1969-1982. Geological Survey of Canada. doi: 10.4095/109253

Adams, J. S., Kraus, M. J., and Wing, S. L. (2011). Evaluating the use of weathering indices for determining mean annual precipitation in the ancient stratigraphic record. *Palaeogeogr. Palaeoclimatol. Palaeoecol.* 309, 358–366. doi: 10.1016/j.palaeo.2011.07.004

Andrews, P., and O'Brien, E. (2010). "Mammal species richness in Africa," in *Cenozoic Mammals*, eds. L. Werdelin, and W. J. Sanders (Berkeley, CA: University of California Press), 921–940.

Andrews, P., and Van Couvering, J. A. (1975). Palaeoenvironments in the East African Miocene. *Approaches Primate Paleobiol.* 5, 62–103.

Ashley, G. M., Beverly, E. J., Sikes, N. E., and Driese, S. G. (2014). Paleosol diversity in the Olduvai Basin, Tanzania: effects of geomorphology, parent material, depositional environment, and groundwater on soil development. *Quatern. Int.* 322, 66–77. doi: 10.1016/j.quaint.2013.12.047

Atchley, S. C., Nordt, L. C., Dworkin, S. I., Ramezani, J., Parker, W. G., Ash, S. R., et al. (2013). A linkage among Pangean tectonism, cyclic alluviation, climate change, and biologic turnover in the Late Triassic: the record from the Chinle Formation, southwestern United States. *J. Sed. Res.* 83, 1147–1161. doi: 10.2110/jsr.2013.89

Banner, J. L., and Hanson, G. N. (1990). Calculation of simultaneous isotopic and trace element variations during water-rock interaction with applications to carbonate diagenesis. *Geochim. Cosmochim. Acta* 54, 3123–3137. doi: 10.1016/0016-7037(90)90128-8

Begun, D. R., Ward, C. V., and Rose, M. D. (1997). "Events in hominoid evolution," in *Function, Phylogeny, and Fossils* (Boston, MA: Springer), 389–415. doi: 10.1007/978-1-4899-0075-3_18

Bishop, W. W., Miller, J. A., and Fitch, F. W. (1969). New potassium-argon age determinations relevant to the Miocene fossil mammal sequence in East Africa. *Am. J. Sci.* 267, 669–699. doi: 10.2475/ajs.267.6.669

Boschetto, H. B., Brown, F. H., and McDougall, I. (1992). Stratigraphy of the Lothidok Range, northern Kenya, and K/Ar ages of its Miocene primates. *J. Hum. Evol.* 22, 47–71. doi: 10.1016/0047-2484(92)90029-9

Brantley, S. L., Goldhaber, M. B., and Ragnarsdottir, K. V. (2007). Crossing disciplines and scales to understand the Critical Zone. *Elements* 3, 307–314. doi: 10.2113/gselements.3.5.307

Bull, W. B. (1991). *Geomorphic Responses to Climate Change*. New York, NY: Oxford University Press.

Cerling, T. E. (1991), Carbon dioxide in the atmosphere: evidence from cenozoic and mesozoic paleosols. *Am. J. Sci.* 291, 377–400. doi: 10.2475/ajs.291.4.377

Couvreur, T. L. P., Chatrou, L. W., Sosef, M. S. M., and Richardson, J. E. (2008). Molecular phylogenetics reveal multiple tertiary vicariance origins of the African rain forest trees. *BMC Biol.* 6, 54–63. doi: 10.1186/1741-7007-6-54

Craig, H. (1965). "The measurements of oxygen isotope palaeo- temperatures," in *Stable Isotopes in Oceanographic Studies and Palaeotemperatures*, ed E. Tongiorgi (Rome: Consiglio Nazionale delle Richerche), 1–24.

Dalrymple, G. B., Alexander, E. C., Lanphere, M. A., and Kraker, G. P. (1981). *Irradiation of Samples for $^{40}Ar/^{39}Ar$ Dating Using the Geological Survey TRIGA Reactor*. Washington, DC: USGS Professional Papers.

Dixey, F. (1944). *Hydrographic Survey of the Northem Frontier District.* Nairobi: Kenya Public Works Department.

Drever, J. I. (1973). The preparation of oriented clay mineral specimens for X-ray diffraction analysis by a filter-membrane peel technique. *Am. Mineralog.* 58, 553–554.

Driese, S. G., Peppe, D. J., Beverly, E. J., DiPietro, L. M., Arellano, L. N., and Lehmann, T. (2016). Paleosols and paleoenvironments of the early Miocene deposits near Karungu, Lake Victoria, Kenya. *Palaeogeogr. Palaeoclimatol. Palaeoecol.* 443, 167–182. doi: 10.1016/j.palaeo.2015.11.030

FAO. (2001). "Lecture notes on the major soils of the world," in *World Soil Resources Report*, eds P. Driessen, J. Deckers, and O. Spaargaren (Food and Agriculture Organization of the United Nations). Available online at: http://www.fao.org/3/a-y1899e.pdf

Farquhar, G. D., Ehleringer, J. R., and Hubick, K. T. (1989). Carbon isotope discrimination and photosynthesis. *Ann. Rev. Plant Biol.* 40, 503–537. doi: 10.1146/annurev.pp.40.060189.002443

Feibel, C. S. (2011). A geologic history of the Turkana Basin. *Evol. Anthropol.* 20, 206–216. doi: 10.1002/evan.20331

Gallagher, T. M., and Sheldon, N. D. (2013). A new paleothermometer for forest paleosols and its implications for Cenozoic climate. *Geology* 41, 647–650. doi: 10.1130/G34074.1

Govindaraju, K. (1994). 1994 compilation of working values and sample description for 383 geostandards. *Geostandards Newsletter* 18, 1–158. doi: 10.1111/j.1751-908X.1994.tb00502.x

Grossman, A., Liutkus-Pierce, C., Kyongo, B., and M'Kirera, F. (2014). New fauna from Loperot contributes to the understanding of early Miocene catarrhine communities. *Int. J. Primatol.* 35, 1253–1274.

Hajek, E. A., and Edmonds, D. A. (2014). Is river avulsion style controlled by floodplain morphology? *Geology* 42, 199–202. doi: 10.1130/G35045.1

Harrison, T. (1982). Small-bodied Apes From the Miocene of East Africa. *Doctoral dissertation, University of London.*

Hendrie, D. B., Kusznir, N. J., Morley, C. K., and Ebinger, C. J. (1994). Cenozoic extension in northern Kenya: a quantitative model of rift basin development in the Turkana area. *Tectonophysics* 236, 409–438. doi: 10.1016/0040-1951(94)90187-2

Hill, A., Nengo, I. O., and Rossie, J. B. (2013). A *Rangwapithecus gordoni* mandible from the early Miocene site of Songhor, Kenya. *J. Hum. Evol.* 65, 490–500. doi: 10.1016/j.jhevol.2013.02.014

Hooijer, D. A. (1971). A new rhinoceros from the late Miocene of Loperot, Turkana District, Kenya. *Bull. Mus. Compar. Zool.* 142, 339–392.

Joubert, P. (1966). *Geology of the Loperot Area. Degree Sheet 18, SE Quarter.* Nairobi: Ministry of Natural Resources, Geological Survey of Kenya.

Klappa, C. F. (1980). Rhizoliths in terrestrial carbonates: classification, recognition, genesis and significance. *Sedimentology* 27, 613–629. doi: 10.1111/j.1365-3091.1980.tb01651.x

Kohn, M. J. (2010). Carbon isotope compositions of terrestrial C3 plants as indicators of (paleo) ecology and (paleo) climate. *Proc. Natl. Acad. Sci. U.S.A.* 107, 19691–19695. doi: 10.1073/pnas.1004933107

Kraus, M. J., and Hasiotis, S. T. (2006). Significance of different modes of rhizolith preservation to interpreting paleoenvironmental and paleohydrologic settings: examples from Paleogene paleosols, Bighorn Basin, Wyoming, USA. *J. Sediment. Res.* 76, 633–646. doi: 10.2110/jsr.2006.052

Kuiper, K. F., Deino, A., Hilgen, F. J., Krijsman, W., Renne, P. R., and Wijbrans, J. R. (2008). Synchronizing rock clocks of earth history. *Science* 320, 500–504. doi: 10.1126/science.1154339

Lewis, D. W., McConchie,D. (1994). *Analytical Sedimentology*. New York, NY: Chapman and Hall. doi: 10.1007/978-1-4615-2636-0

Liutkus-Pierce, C. M., Takashita-Bynum, K., Beane, L. A., Edwards, E., Burns, O. E., Mana, S., et al. (2017). *Data from: Ar-Ar results for Loperot, Kenya*. Mendeley Data (2017). doi: 10.17632/ff7yz7jzsy.1

Lukens, W. E., Lehmann, T., Peppe, D. J., Fox, D. L., Driese, S. G., and McNulty, K. P. (2017). The early miocene critical zone at Karungu, Western Kenya: an equatorial, open habitat with few primate remains. *Front. Earth Sci.* 5:87. doi: 10.3389/feart.2017.00087

Mack, G. H., and James, W. C. (1994). Paleoclimate and the global distribution of paleosols. *J. Geol.* 102, 360–366. doi: 10.1086/629677

Maglio, V. J. (1969). *A Shovel-Tusked Gomphothere From the Miocene of Kenya*. Cambridge, MA: Breviora.

Marshall, J. D., Brooks, J. R., and Lajtha, K. (2007). Sources of variation in the stable isotopic composition of plants. *Stable Isotopes Ecol. Environ. Sci.* 2, 22–60. doi: 10.1002/9780470691854.ch2

Maxbauer, D.P, Peppe, D. J., Bamford, M., McNulty, K. P., Harcourt-Smith, W. E. H., and Davis, L. E. (2013). A morphotype catalog and paleoenvironmental interpretations of early Miocene fossil leaves from the Hiwegi Formation, Rusinga Island, Lake Victoria, Kenya. *Palaeontol. Electron.* 16:28A. doi: 10.26879/342

Mead, J. G. (1975). A fossil beaked whale (Cetacea: Ziphiidae) from the Miocene of Kenya. *J. Paleontol.* 49, 745–751.

Miller, E., Benefit, B., McCrossin, M., Plavcan, J., Leakey, M., El-Barkooky, A., et al. (2009). Systematics of early and middle Miocene Old World monkeys. *J. Hum. Evol.* 57, 195–211. doi: 10.1016/j.jhevol.2009.06.006

Min, K. W., Mundil, R., Renne, P. R., and Ludwig, K. R. (2000). A test for systematic errors in $^{40}Ar/^{39}$ Ar geochronology through comparison with U/Pb analysis of a 1.1-Ga rhyolite. *Geochim. Coscmochim. Acta* 64, 73–98. doi: 10.1016/S0016-7037(99)00204-5

Moore, D. M., and Reynolds, R. C. Jr. (1997). *X-ray Diffraction and the Identification and Analysis of Clay Minerals*. New York, NY: Oxford University Press.

Morgan, M. E., Kingston, J. D., and Marino, B. D. (1994). Carbon isotopic evidence for the emergence of C4 plants in the Neogene from Pakistan and Kenya. *Nature*. 367, 162–165. doi: 10.1038/367162a0

Morley, C. K., Ngenoh, D. K., and Ego, J. K. (1999a). "Introduction to the East African Rift System," in *Geoscience of the Rift Systems-Evolution of East Africa*, ed C. K. Morley (Tulsa, OK: AAPG Studies in Geology), 1–18.

Morley, C. K., Wescott, W. A., Stone, D. M., Harper, R. M., Wigger, S. T., Day, R. A., et al. (1999b). "Geology and geophysics of the western Turkana Basins," in *Geoscience of the Rift Systems-Evolution of East Africa*, ed. C. K. Morley (Tulsa, OK: AAPG Studies in Geology), 19–54.

Munsell Color. (2010). *Munsell Soil Color Charts: With Genuine Munsell Color Chips*. Grand Rapids, MI.

Nadeau, P. H., Wilson, M. J., McHardy, W. J., and Tait, J. M. (1985). The conversion of smectite to illite during diagenesis: evidence from some illitic clays from bentonites and sandstones. *Mineral. Mag.* 49, 393–400. doi: 10.1180/minmag.1985.049.352.10

Nordt, L. C., and Driese, S. G. (2013). Application of the critical zone concept to the deep-time sedimentary record. *Sediment. Record* 11, 4–9. doi: 10.2110/sedred.2013.3.4

Passey, B. H. (2012). Reconstructing terrestrial environments using stable isotopes in fossil teeth and paleosol carbonates. *Paleontol. Soc. Papers* 18, 167–194. doi: 10.1017/S1089332600002606

Peppe, D. J., Deino, A. L., Driese, S. G., Fox, D. L., Kingston, J. D., Kinyanjui, R. N., et al. (2017). "Early miocene paleoclimate and paleoenvironments across East Africa," in *GSA Annual Meeting*, Vol. 49, (Seattle, WA: Geological Society of America Abstracts with Programs). doi: 10.1130/abs/2017AM-304937

Peppe, D. J., Deino, A. L., Mcnulty, K. P., Lehmann, T., Harcourt-Smith, W. E., Dunsworth, H. M., et al. (2011). New age constraints on the early Miocene faunas from Rusinga and Mfangano Islands (Lake Victoria, Kenya). *Am. J. Phys. Anthropol.* 144:237.

Pickford, M. (1995). Fossil land snails of East Africa and their palaeoecological significance. *J. Afr. Earth Sci.* 20, 167–226. doi: 10.1016/0899-5362(95)94397-R

Reed, K. E. (1997). Early hominid evolution and ecological change through the African Plio-Pleistocene. *J. Hum. Evol.* 32, 289–322. doi: 10.1006/jhev.1996.0106

Retallack, G. J. (1990). *Soils of the Past: An Introduction to Paleopedology*. Oxford: Blackwell Science, Ltd.

Retallack, G. J. (2001). *Soils of the Past: An Introduction to Paleopedology*, 2nd edition. Oxford: Blackwell Science, Ltd.

Retallack, G. J., Wynn, J. G., Benefit, B. R., and McCrossin, M. L. (2002). Paleosols and paleoenvironments of the middle Miocene, Maboko Formation, Kenya. *J. Hum. Evol.* 42, 659–703. doi: 10.1006/jhev.2002.0553

Rossie, J. B., and Seiffert, E. R. (2006). "Continental paleobiogeography as phylogenetic evidence," in *Primate Biogeography*, eds S. M. Lehman and J. Fleagle (New York, NY: Springer), 469–522.

Royer, D. L., Donnadieu, Y., Park, J., Kowalczyk, J., and Goddéris, Y. (2014). Error analysis of CO2 and O2 estimates from the long-term geochemical model GEOCARBSULF. *Am. J. Sci.* 314, 1259–1283. doi: 10.2475/09.2014.01

Sheldon, N. D., Retallack, G. J., and Tanaka, S. (2002). Geochemical climofunctions from North American soils and application to paleosols across the Eocene-Oligocene boundary in Oregon. *J. Geol.* 110, 687–696. doi: 10.1086/342865

Sheldon, N. D., and Tabor, N. J. (2009). Quantitative paleoenvironmental and paleoclimatic reconstruction using paleosols. *Earth-Sci. Rev.* 95, 1–52. doi: 10.1016/j.earscirev.2009.03.004

Steiger, R. H., and Jager, E. (1977). Subcommission on geochronology: convention on the use of decay constants in geo- and cosmochronology. *Earth Planet Sci. Lett.* 36, 359–362. doi: 10.1016/0012-821X(77)90060-7

Stevens, N. J., Seiffert, E. R., O'Connor, P. M., Roberts, E. M., Schmitz, M. D., Krause, C., et al. (2013). Palaeontological evidence for an Oligocene divergence between Old World monkeys and apes. *Nature* 497, 611–614. doi: 10.1038/nature12161

Szarek, S. R., and Troughton, J. H. (1976). Carbon isotope ratios in crassulacean acid metabolism plants: seasonal patterns from plants in natural stands. *Plant Physiology* 58, 367–370. doi: 10.1104/pp.58.3.367

Talbot, M. R., Morley, C. K., Tiercelin, J.-J., Le Herisse, A., Potdevin, J.-L., and Le Gall, B. (2004). Hydrocarbon potential of the Meso-Cenozoic Turkana Depression, northern Kenya. II. source rocks: quality, maturation, depositional environments and structural control. *Marine Petrol. Geol.* 21, 63–78. doi: 10.1016/j.marpetgeo.2003.11.008

Tiercelin, J.-J., Potdevin, J.-L., Morley, C. K., Talbot, M. R., Bellon, H., Rio, A., et al. (2004). Hydrocarbon potential of the Meso-Cenozoic Turkana Depression, northern Kenya. I., Reservoirs: depositional environments, diagenetic characteristics, and source rock-reservoir relationships. *Mar. Petrol. Geol.* 21, 41–62. doi: 10.1016/j.marpetgeo.2003.11.007

Tipple, B. J., Meyers, S. R., and Pagani, M. (2010). Carbon isotope ratio of Cenozoic CO_2: a comparative evaluation of available geochemical proxies. *Paleoceanogr. Paleoclimatol.* 25. doi: 10.1029/2009PA001851

Uno, K. T., Polissar, P. J., Jackson, K. E., and deMenocal, P. B. (2016). Neogene biomarker record of vegetation change in eastern Africa. *Proc. Natl. Acad. Sci. U.S.A.* 113, 6355–6363. doi: 10.1073/pnas.1521267113

Urban, M. A., Nelson, D. M., Jiménez-Moreno, G., Châteauneuf, J.-J., Pearson, A., and Hu, F. S. (2010). Isotopic evidence of C_4 grasses in southwestern Europe during the early Oligocene–Middle Miocene. *Geology* 38, 1091–1094. doi: 10.1130/G31117.1

Velde, B., and Barré, P. (2009). *Soils, Plants and Clay Minerals: Mineral and Biologic Interactions*. New York, NY: Springer.

Vincens, A., Tiercelin, J-J., and Buchet, G. (2006). New Oligocene-early Miocene microflora from the southwestern Turkana Basin: Paleoenvironmental implications in northern Kenya Rift. *Palaeogeogr. Palaeoclimatol. Palaeoecol.* 239, 470–486. doi: 10.1016/j.palaeo.2006.02.007

Wichura, H., Jacobs, L. L., Lin, A., Polcyn, M. J., Manthi, F. K., Winkler, D. A., et al. (2015). A 17-My-old whale constrains onset of uplift and climate change in east Africa. *Proc. Natl. Acad. Sci. U.S.A.* 112, 3910–3915. doi: 10.1073/pnas.1421502112

Wright, V. P. (1990). "A micromorphological classification of fossil and recent calcic and petrocalcic microstructures," in *Soil Micromorphology: A Basic and Applied Science*, ed L. A. Douglas (Amsterdam: Elsevier), 401–407.

Wynn, J. G. (2000). Paleosols, stable carbon isotopes, and paleoenvironmental interpretation of Kanapoi, Northern Kenya. *J. Hum. Evol.* 39, 411–432. doi: 10.1006/jhev.2000.0431

Conflict of Interest Statement: The authors declare that the research was conducted in the absence of any commercial or financial relationships that could be construed as a potential conflict of interest.